Ultrafine Aerosol Deposition in Planar Channel Flow

by

Michael Yuan Feng

Submitted to the Department of Mechanical Engineering
in partial fulfillment of the requirements for the degree of

Bachelor of Science in Mechanical Engineering

at the

MASSACHUSETTS INSTITUTE OF TECHNOLOGY

May 1994

Author .....
Department of Mechanical Engineering
May 6, 1993

Certified by .....
John H. Lienhard V
Associate Professor
Thesis Supervisor

Accepted by .....
Peter Griffith
Chairman, Departmental Committee on Undergraduate Students

Acknowledgments

First and foremost, I would like to thank my parents. My father, who graduated from the MIT of China, Qinghua University, always served as an inspiration to enter the engineering field. To my mom, who has given me all the love and affection a son could want, thanks. I know you wanted me to go Course 6-1, so I hope this thesis makes you proud of giving me the chance to choose mechanical engineering.

Of course, none of this would not have happened if Professor John H. Lienhard V had not hired me in the summer of 1992 to do this project as a UROP. At that time, I was anxious to try my mechanical engineering skills, and I am extremely grateful he gave me the chance to prove myself. As a result, I have found my niche in mechanical engineering and love every moment. Besides supervising my thesis, he has taught me 2.671 and 2.51 and done an excellent job. In my opinion, he is one of the best lecturers in mechanical engineering. I will always remember fondly how a soldering iron was modelled as a fin in heat transfer! So, thanks to the man who has most influenced my undergraduate education at MIT.

Thanks also go to Kurt W. Roth '89 who made my UROP experience infinitely more enjoyable and contributed invaluable time and energy to this thesis. I do not think I could have had a better boss from the many uncanny imitations of the faculty at MIT to the answering of innumerable questions(except for piezometric head). I hope this thesis contributes in some way to his own doctoral thesis.

I would also like to thank Mr. James Grinnell, director of the CAD lab in the Martin Center for Design in the department of mechanical engineering. He graciously permitted access to the scanner.

Finally, with regahds to cawfee, I cannot forget Michael P. Frongillo, our man at the microscopy facility. I shall drink *Eight O'Clock* coffee from now until eternity.

This research has been supported in part by the National Institute of Health.

Ultrafine Aerosol Deposition in Planar Channel Flow

by

Michael Yuan Feng

Submitted to the Department of Mechanical Engineering
on May 6, 1993, in partial fulfillment of the
requirements for the degree of
Bachelor of Science in Mechanical Engineering

Abstract

A technique was developed for measuring the deposition of aerosols from 0.01 to $1\mu m$ diameter in a turbulent, planar channel flow. The ultimate goal of this project was to investigate ultrafine aerosol deposition in lung passageways.

A procedure was developed to measure ultrafine aerosol deposition in a turbulent planar channel. Titanium tetrachloride, $TiCl_4$, reacting with atmospheric water vapour created a polydisperse titanium dioxide, TiO_2, aerosol which was injected into the flow. The aerosol deposited on electron microscope grids mounted on the bottom of a test section. Then the grids were photographed at 20,000 magnification with a transmission electron microscope, and a digital image analysis computer program counted and sized the particles on the grids.

Two sets of tests were performed using slightly different apparatuses. An initial battery of tests was performed the summer of 1992. Then another battery of tests was run in the spring of 1993 incorporating many design improvements to the apparatus. Both tests had a step upstream of the grids to study the effects of secondary flows, a common occurrence in the lung.

The data taken during the summer of 1992 showed five times greater deposition within the secondary flow than before the step. Deposition at the reattachment point of the flow was still higher than the non-secondary flow case, but lower than within the secondary flow itself. It has been surmised that the vortex in the secondary flow entrained the smaller particles and brought them much closer to the bottom of the wall. This created a higher concentration gradient to drive mass transfer.

The data taken during the spring of 1993 showed that the secondary flows inhibited mass transfer. Within the secondary flow deposition only reached 10 percent of what was attained upstream of the step. It was concluded that the secondary flow was affected by the design changes which caused the diffusive boundary layer to be too thick for enhanced mass transfer to occur. However, the sample size was much smaller in 1993 than in 1992, so further testing should be conducted.

Thesis Supervisor: John H. Lienhard V
Title: Associate Professor

Ultrafine Aerosol Deposition in Planar Channel Flow

by

Michael Yuan Feng

Submitted to the Department of Mechanical Engineering
on May 6, 1993, in partial fulfillment of the
requirements for the degree of
Bachelor of Science in Mechanical Engineering

Abstract

A technique was developed for measuring the deposition of aerosols from 0.01 to $1\mu m$ diameter in a turbulent, planar channel flow. The ultimate goal of this project was to investigate ultrafine aerosol deposition in lung passageways.

A procedure was developed to measure ultrafine aerosol deposition in a turbulent planar channel. Titanium tetrachloride, $TiCl_4$, reacting with atmospheric water vapour created a polydisperse titanium dioxide, TiO_2, aerosol which was injected into the flow. The aerosol deposited on electron microscope grids mounted on the bottom of a test section. Then the grids were photographed at 20,000 magnification with a transmission electron microscope, and a digital image analysis computer program counted and sized the particles on the grids.

Two sets of tests were performed using slightly different apparatuses. An initial battery of tests was performed the summer of 1992. Then another battery of tests was run in the spring of 1993 incorporating many design improvements to the apparatus. Both tests had a step upstream of the grids to study the effects of secondary flows, a common occurrence in the lung.

The data taken during the summer of 1992 showed five times greater deposition within the secondary flow than before the step. Deposition at the reattachment point of the flow was still higher than the non-secondary flow case, but lower than within the secondary flow itself. It has been surmised that the vortex in the secondary flow entrained the smaller particles and brought them much closer to the bottom of the wall. This created a higher concentration gradient to drive mass transfer.

The data taken during the spring of 1993 showed that the secondary flows inhibited mass transfer. Within the secondary flow deposition only reached 10 percent of what was attained upstream of the step. It was concluded that the secondary flow was affected by the design changes which caused the diffusive boundary layer to be too thick for enhanced mass transfer to occur. However, the sample size was much smaller in 1993 than in 1992, so further testing should be conducted.

Thesis Supervisor: John H. Lienhard V
Title: Associate Professor

Contents

List of Figures

List of Tables

Chapter 1

Introduction

1.1 Project Motivation

This project started as a feasibility study of experimental methods to measure ultrafine particle deposition to be submitted as a grant proposal to the National Institute of Health (NIH). NIH's interest in the project was the possibility to model the deposition of airborne particulates in the lung passageways. Many airborne particulates that enter the lung are known to be mutagenic, i.e. capable of producing genetic damage that can lead to cancer[11]. On the other hand, inhalers deliver medicine to the lungs in an aerosol form, so knowledge of where the medicine deposits is beneficial.

1.2 The Definition of "Ultrafine" Aerosol Particles

In response, researchers have studied aerosol deposition intensely, but most research has involved particle sizes greater than one micron[11]. On the other hand, urban air pollution is composed of particles that are generally much smaller than one micron[11]. For example, soot particles have an aerodynamic diameter between $0.01\mu m$ and $0.5\mu m$[11]. It has also been demonstrated that particles of approximately $0.1\mu m$ are the greatest contributor to the total surface area of normal urban aerosols thereby

transporting surface-absorbed mutagens to lung tissues most efficiently[11]. Naturally, more attention should be paid to understanding how these potentially harmful aerosols are transported within the lungs. For the purposes of this thesis, "ultrafine" means less than one micron in particle diameter.

1.3 Previous Ultrafine Aerosol Analysis

In the past, simple theories and extrapolations from data on large diameter particles were employed to predict deposition of ultrafine aerosols[11]. For example, Fuchs's expression for deposition due to simultaneous gravitational settling and diffusion is simply an addition of the two mechanisms[7, p. 251].However, these predictions tend to be much lower than actual results[11]. The first assumption most deposition models make is unidirectional flow, i.e. no secondary flows, but secondary flows are known to exist at the tracheobronchial bifurcations. The second assumption is that the only mechanism for ultrafine deposition is brownian diffusion. This assumption ignores other forces that may enhance deposition rates, e.g. gravitational settling or inertial impaction.

1.4 The Goals of this Project

The purpose of this thesis is two-fold: to develop a method to accurately measure ultrafine particle deposition and then analyze the results. The development of measurement techniques of ultrafine aerosol deposition in this planar channel flow might lead to studying deposition in more complex flows such as curving flows or flows around bifurcations to model the lung more accurately. The results of this thesis compare the deposition in turbulent pipe flow to deposition in a secondary flow. I hope to demonstrate that current predictions on ultrafine aerosol deposition in secondary flows are inadequate.

Chapter 2

Theory

2.1 Aerosol Deposition Mechanisms in the Lung

The three basic mechanisms of deposition in the lung are inertial impaction, gravitational sedimentation, and diffusive (brownian) deposition[8]. Impaction occurs in flows with curvilinear motion. Deposition occurs because the particles want to continue in a straight line due to inertia, so they separate from the streamlines of the flow causing them to impact on the airway walls. Impaction is normally found in the upper airways because of the high number of direction changes in the flow and the higher flow rates. Sedimentation has its greatest effect in smaller airways(e.g. alveolar region) where the velocity of the flow is low and the airway dimension is small. Sedimentation is the result of gravity acting on larger particles' masses. Brownian motion is the random motion produced by collision with gas molecules. Aerosol particles exhibit strong Brownian motion when their diameters are small. The random motion causes deposition in narrow passageways when particles collide with the wall. The relative significance of deposition mechanisms to each other depends greatly on particle size.

2.1.1 Inertial Impaction

According to Friedlander[5], the effect of inertial impaction is most important for particles larger than $1\mu m$. Deposition by this mechanism occurs when the carrier flow changes direction because the inertia of heavier particles prevents the particle from following the flow streamlines and causes it to impact against the bounding wall.

2.1.2 Gravitational Settling

Gravity deposits heavier particles, i.e. larger particles. Friedlander [5] quantifies this with an expression for the terminal settling velocity, V_{ts}, for a particle in stagnant air. He derives it by balancing the gravitational force field and the drag on the particle:

$$\mathbf{c} = \frac{\mathbf{F}}{f} \tag{2.1}$$

where $\mathbf{c}$ is the velocity vector, $\mathbf{F}$ is the force vector, and f is the friction coefficient. After substituting a gravitational field for the force field[5, p. 35],

$$V_{ts} = \frac{\rho_p g d_p^2}{18\mu} C[1 - \frac{\rho}{\rho_p}] \tag{2.2}$$

- ρ = gas density
- ρ_p = particle density
- g = gravitational acceleration, $9.8m/s^2$
- μ = gas viscosity (air)
- d_p = particle diameter

C is the Cunningham slip correction which is determined by:

$$C = 1 + \frac{\lambda}{d_p}[2.514 + 0.800exp(-0.55\frac{d_p}{\lambda})] \tag{2.3}$$

λ is the mean free path of the gas which for air is $.066\mu m$ at $20°C$. C becomes significant when $d_p \sim \lambda$ which is the case for ultrafine aerosols.

Although the equation for V_{ts} is for a still gas, it does give the relationship between the terminal settling velocity and the particle diameter:

$$V_{ts} \propto d_p \tag{2.4}$$

As d_p decreases so does the gravitational settling rate.

2.1.3 Brownian Diffusion

Aerosol particles undergo random, wiggling motions in air called Brownian motion. When there is a concentration gradient of the aerosol then the Brownian motion causes net transport of these particles from the region of high concentration to low concentration which is called diffusion. The diffusion process can be characterized by the particle diffusion coefficient, $\mathcal{D}$[10].

$$\mathcal{D} = C\frac{k_B T}{\mu_{air} 3\pi d_p} \tag{2.5}$$

The larger $\mathcal{D}$ is the more Brownian motion, i.e. diffusion.

To obtain a rough idea of how settling and diffusion vary with particle diameter table 2.1 has been reproduced from *Aerosol Technology* by William C. Hinds[8, p. 145].

2.2 Convective Deposition in Turbulent Flow

In a turbulent pipe flow, small particles deposit on the walls by entrainment in the turbulent eddies and Brownian diffusion. Analysis of deposition by convective diffusion first requires a characterization of the flow field. The flow is divided into three different zones illustrated in figure 2-1 reproduced from page 78 of *Smoke Dust and Haze* by Friedlander[5]. In the turbulent core, Brownian diffusion is negligible compared with transport by the turbulent eddies. Closer to the wall, Brownian and eddy diffusion are equally significant. Finally, adjacent to the wall, there is a thin viscous

Diameter (μm)	Cumulative Deposition		Ratio, $\frac{\text{Diffusion}}{\text{Settling}}$
	Diffusion (number/cm^2)	Settling (number/cm^2)	
0.001	2.5	6.5×10^{-5}	3.8×10^{4}
0.01	0.26	6.7×10^{-4}	390
0.1	2.9×10^{-2}	8.5×10^{-3}	3.4
1.0	5.9×10^{-3}	0.35	1.7×10^{-2}
10	1.7×10^{-3}	31	5.5×10^{-5}
100	5.5×10^{-4}	2500	2.2×10^{-7}

[a]This assumes an aerosol concentration of 1 particle/cm^3 outside the gradient region.

Table 2.1: Cumulative Deposition of Unit-Density Particles onto a Horizontal Surface from Unit Aerosol Concentration during 100 seconds by Diffusion and Gravitational Settling.

sublayer where turbulent fluctuations are weak. However, for $Sc \gg 1$ even these weak fluctuations bring the particles closer to the wall before Brownian diffusion can act[5].

Hinds [8] provides an empirical formula for predicting aerosol deposition in turbulent pipe flow. He assumes a constant concentration, n_o, outside of the thin viscous sublayer adjacent to the wall and zero concentration at the wall. The thickness of the diffusive layer (from wall to n_o), δ, was derived by Fuchs[7, p. 269]:

$$\delta = \frac{28.5 d_h \mathcal{D}^{\frac{1}{4}}}{Re^{\frac{7}{8}} (\mu/\rho)^{\frac{1}{4}}} \tag{2.6}$$

- d_h = hydraulic diameter of duct
- Re = Reynolds number = $\frac{\rho U d_h}{\mu}$

Using δ, the downward velocity,V_{dep}, of any particle can be determined from[8, p. 147]:

$$V_{dep} = \frac{\mathcal{D}}{\delta} \tag{2.7}$$

By the definition of V_{dep}, it can be shown that:

$$V_{dep} = \frac{J}{n_o} \tag{2.8}$$

where J is the mass flux towards the wall.

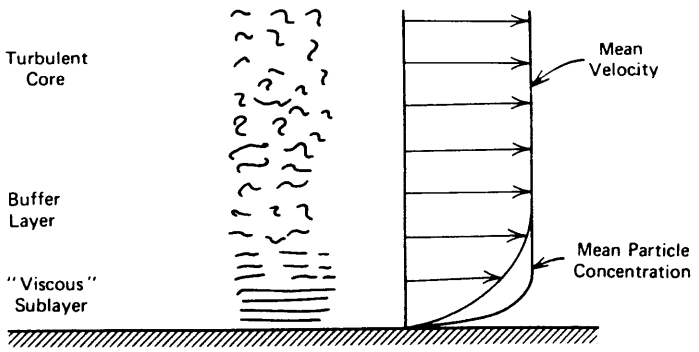

Figure 2-1: Schematic Diagram Showing the Structure of Turbulent Pipe Flow.

It is also useful to calculate what percentage of the initial concentration escapes deposition and leaves the tube. Hinds gives an expression for this, too [8, p. 148]:

$$\frac{n_{out}}{n_{in}} = exp(\frac{-4V_{dep}L}{d_h\bar{U}}) \tag{2.9}$$

where L is the tube length.

2.3 Secondary Flows

A secondary flow was created by placing a step block in the flow. This obstacle causes the shear flow to separate off the top of the obstacle. After passing the obstacle, the separated shear layer curves sharply downstream in the reattachment region. Part of the separated flow becomes entrained upstream into a recirculation zone by a strong adverse pressure gradient. Unfortunately, most data on sudden blockages to flows refers to backward facing steps or blunt plates [3](see figure 2-2 reproduced from Eaton and Johnston's paper[3].) For backward facing steps, reattachment lengths for turbulent flow are independent of Reynold's number[3]. From Eaton, the dimensionless ratio of reattachment length to step height, x_r/h_{step} is approximately six[3]. However, J. Faramarzi and E. Logan [4] recently studied reattachment lengths behind a single roughness element (similar to the forward-backward facing step employed here, see figure 2-3 reproduced from Faramarzi and Logan's paper[4]). They

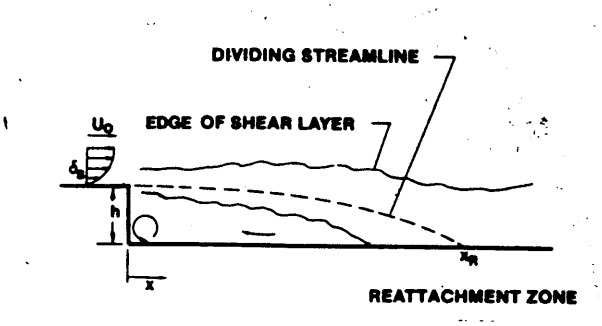

Figure 2-2: Backward Facing Step.

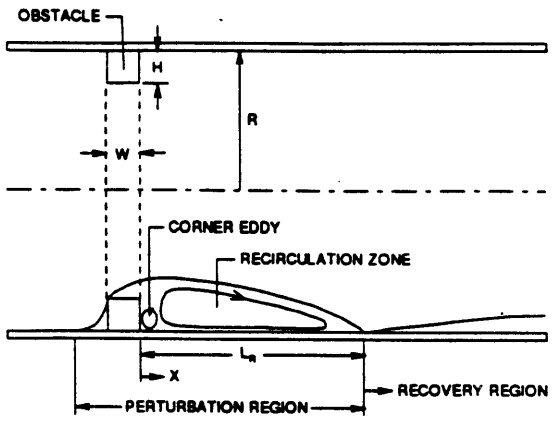

Figure 2-3: Forward-Backward Facing Step.

used a circular pipe with a ring-shaped element of square cross-section fitted against the entire inside perimeter of the pipe. The present channel only has the obstacle fitted along the bottom wall(see figure 3-1.)

By examining the difference in results between the two cases, it can be concluded that the ratio of length of obstacle to height of obstacle is important in determining the reattachment length. The length of the obstacle gives the flow time to reduce the vertical velocity component, i.e. stop it from moving away from the wall. Thus, the backward facing step has a much lower reattachment length than a forward-backward facing step, particularly when the step height is equal to the step length. The reattachment length for a forward-backward step converges with the backward-

facing case when the step length increases to approximately twice the step height.

Adapting my channel configuration, to the results of Faramarzi and Logan via a hydraulic diameter, the reattachment length is predicted to be approximately nine step heights.

2.4 The Effects of Secondary Flows on Deposition

Within the past twenty years, researchers have discovered the compounding effect of concurrent deposition mechanisms[11]. Inertial deposition, in particular, has been found to enhance deposition by brownian diffusion and gravitational settling. This is especially important for ultrafine aerosols where the inertia of the particles is generally regarded as negligible. The concurrent deposition mechanisms differ significantly from simple superposition of inertial deposition on Brownian or gravitational deposition. This is because inertial effects concentrate particles in regions of high strain or low vorticity, e.g. secondary flows[11].

A study by Maxey [12] examined the influence of inertia on gravitational settling in a turbulent flow. He demonstrated that inertia concentrates particles in regions of high strain rate or low vorticity, thus enhancing deposition. In this way, gravitational settling rose by more than 25% for minimal inertial effects.

Similar to the present test flow, Kim et. al.[9] examined deposition behind a step in a pipe flow for much larger particles and obtained deposition rates up to 100 times greater than without a step. He attributed the two orders of magnitude increase in deposition to recirculating vortices and added turbulence created by the step.

Although inertia and diffusive effects are weak, the compounding effects of inertia are likely to be significant in secondary flows. At high Schmidt number, $Sc = \frac{\nu}{\mathcal{D}}$, (the case for ultrafine aerosol particles), the diffusive layer next to the wall is extremely thin. The weak inertial effects compress the aerosol at the outer edge of the diffusive layer creating a much higher concentration gradient to drive mass transfer, i.e. inertia can increase deposition[11].

Chapter 3

Apparatus

3.1 Wind Tunnel

The wind tunnel produced a turbulent channel flow with an upstream air supply, an aerosol seeding source, and various flow manipulators which fed a narrow planar channel test section. See figure 3-1.

3.1.1 Flow Manipulators

The flow manipulators served to create a uniform concentration of aerosol and of course, the turbulent flow desired. Downstream of the injection there was a grid to cause turbulence which mixed the aerosol. Mixing the aerosol created the constant bulk concentration in the center of the channel. A diffuser section between the compressor and the channel widened the flow to the width of the test section and reduced any time-varying turbulence caused by the compressor. Caution should be taken in the angle of diffusion so that flow does not separate from the side walls [14, p.356]. Next, a honeycomb matrix straightened the flow, and the contraction downsized the flow's cross-sectional area to that of the test section. At the beginning of the test section, sandpaper 3.1 tripped the flow to ensure quick transition to turbulence. A step was also glued to the bottom of the test section to induce secondary flows. A diagram of the wind tunnel is given in figure 3-1.

Test Date	1992	1993
Honeycomb Hole Diameter	$0.6cm$	$0.6cm$
Hydraulic Diameter, d_h	$2.345cm$	2.345
Maximum Centerline Velocity, $\bar{U}$	$2.76m/s$	$2.2m/s$
Reynolds Number, Re_{d_h}	5000	3568
Sandpaper Grit	36-grit	36-grit

Table 3.1: Hydrodynamic Properties of Wind Tunnel.

3.1.2 Aerosol Injection

The aerosol was injected through a hole on the top of the section adjacent to the compressor. Injecting the aerosol far upstream of the test section allowed more aerosol to form and to mix. A more detailed discussion of the aerosol seeding follows in the proceeding section.

3.1.3 Experimental Protocol Considerations

The entire assembly of flow manipulators and test section was constructed of Lexan to resist corrosion and to provide a clear view of the aerosol-seeded flow. The top of the test section was also removable to allow easy access for deposition measurements.

3.2 Aerosol Seeding

Titanium dioxide was chosen as the aerosol because titanium tetrachloride can be exposed to air to form titanium dioxide smoke quickly and cheaply. For these reasons, researchers often use titanium dioxide for flow visualization. However,the air-sensitivity of the liquid titanium tetrachloride, $TiCl_4$, requires a system closed to atmospheric air.

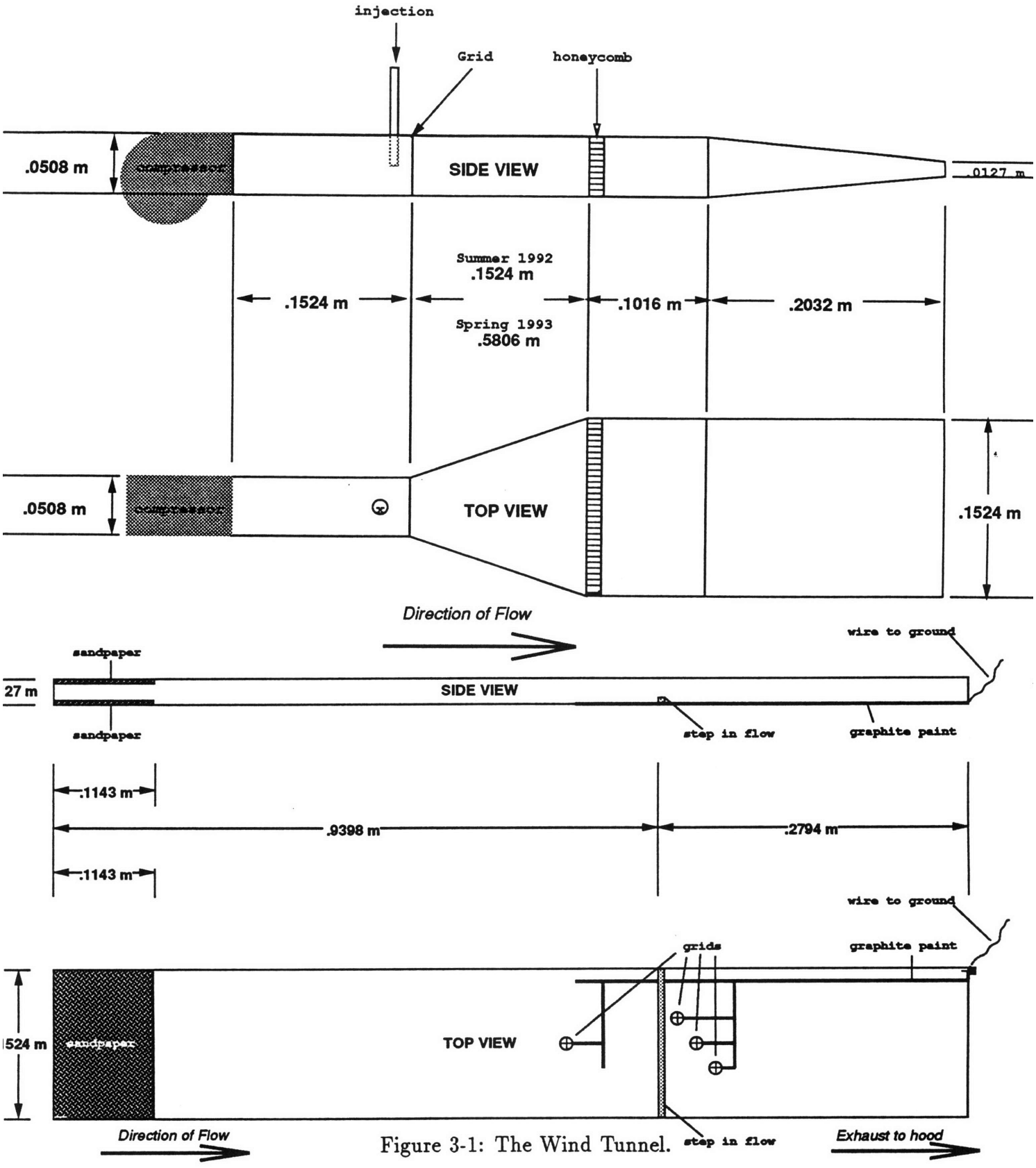

Figure 3-1: The Wind Tunnel.

3.2.1 Handling $TiCl_4$

Attention should also be brought to the products of the reaction between titanium tetrachloride and water given in equation 3.1.

$$TiCl_4 + 2H_2O \rightarrow TiO_2 + 4HCl \tag{3.1}$$

The presence of hydrochloric acid in the flow meant that all metal in the flow would be corroded. Thus, metal objects inside the wind tunnel were coated with acid-resistant material and leaks sealed with plasticene or silicone sealant. The aerosol exiting the test section exhausted into a fume hood to prevent contaminating the laboratory.

The short reaction time of $TiCl_4$ also meant that any residual $TiCl_4$ left in syringe needles or cannula tended to clog these small-diameter (20-gauge) tubes with TiO_2. Commercial cleaners for syringe needles are available which inject solvent at high pressures into the clogged needles to remove inner residue, but during the course of experiments soaking the needles or cannula in denatured alcohol worked just as well. For faster cleaning, I filled a syringe with alcohol and injected it into the clogged tube with a smaller diameter needle. Because much time was wasted cleaning needles, larger diameter needles were recommended although not tried.

For personal protection, acid-resistant covering is highly recommended. Whenever handling $TiCl_4$, the experimenter should wear a disposable lab coat, full-size goggles, and disposable rubber gloves. The potential hazards of handling $TiCl_4$ *should not be underestimated.*

3.2.2 Particle Size Distribution of Aerosol

Figure 3-2 reprinted from Freymuth, et. al. [13] shows a particle size distribution of a TiO_2 aerosol. Notice the aerosol is polydisperse with most particles falling in the $.5\mu m$ range (From section A.4, aerodynamic diameter is approximately twice the geometric diameter for TiO_2). This size distribution is of the bulk concentration, n_o, not of the concentration deposited on the wall. This graph is also *not* generally the case; however, lacking a particle size distribution of the concentrations used, this particle

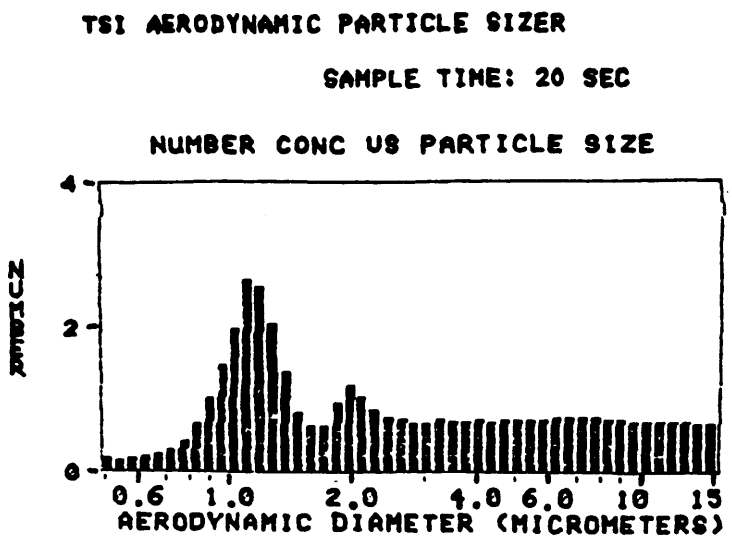

Figure 3-2: Particle Size Distribution for TiO_2 Aerosol.

size distribution has been substituted. Of course, the size distribution will probably depend on local atmospheric conditions and the injection system used. Figure 3-2 merely confirms the possibility of obtaining ultrafine aerosols from TiO_2.

3.2.3 Injection Technique

Rubber septa were fitted to the bottle of $TiCl_4$ and the $10mL$ buret to allow air-proof access via syringe needles and cannula (double-tipped syringe needles) which kept out water vapor. Then pressurized inert gases such as nitrogen could be pumped in through a syringe needle to force the $TiCl_4$ liquid to move from vessel to vessel, again under air-tight conditions.

Before any $TiCl_4$ was transported, nitrogen gas at five to ten psi purged the entire system of atmospheric air. The nitrogen entered the bottle of $TiCl_4$, continued through to the buret, and then exited out of a gas bubbler. The gas bubbler was a piece of glass hardware that allowed gas under pressure to bubble out through a dense liquid such as mercury or mineral oil but prevented atmospheric air from entering (see figure 3-4 reproduced from an Aldrich Chemical catalog) [1]. See figure 3-3 for a schematic diagram of the system in purge mode.

After purging for five to ten minutes, I started filling the buret with $TiCl_4$ liquid (see figure 3-5. This was done by inserting the $TiCl_4$ end of the cannula into the

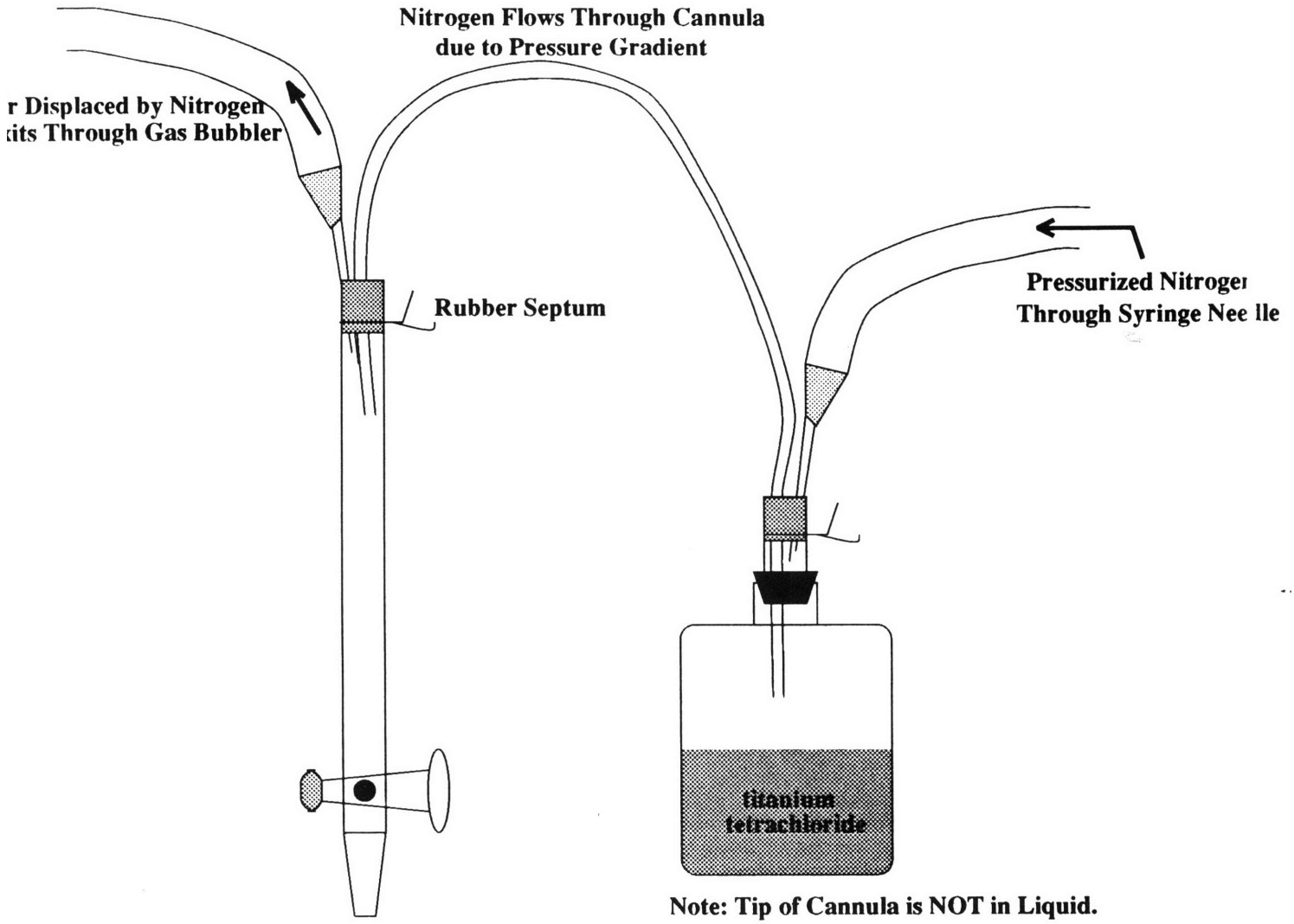

Figure 3-3: Configuration to Purge Aerosol Seeding System.

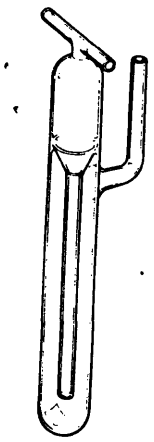

Figure 3-4: Typical Gas Bubbler.

liquid. The pressure from the nitrogen gas forced the liquid up the cannula and into the buret. After filling up the buret, the $TiCl_4$ end of the cannula was withdrawn from the liquid returning the system to the purge mode.

Aerosol could now be created by opening the buret stopcock. The $TiCl_4$ was dripped into the top of the tunnel through a hole approximately $2mm$ in diameter where it formed the TiO_2 aerosol with the passing air within a few seconds. To contain the aerosol, plasticene filled in the gaps between the hole and the buret. See figure 3-6 for a schematic diagram of the system in the injection mode.

3.3 Transmission Electron Microscopy (TEM)

Transmission electron microscopy was employed because of its highly localized measurements and its ability to resolve ultrafine particle sizes with high contrast. Upon consultation with an experienced electron microscopist [15], I selected 200 mesh tabbed grids with a thin Formvar film covered with a light layer of carbon produced by Ted Pella, Inc. The Formvar coating prevented particles from falling through the grids, and the carbon provided excellent electrical conducting properties to eliminate electrical charging effects on deposition. The tabs on the grids also provided conve-

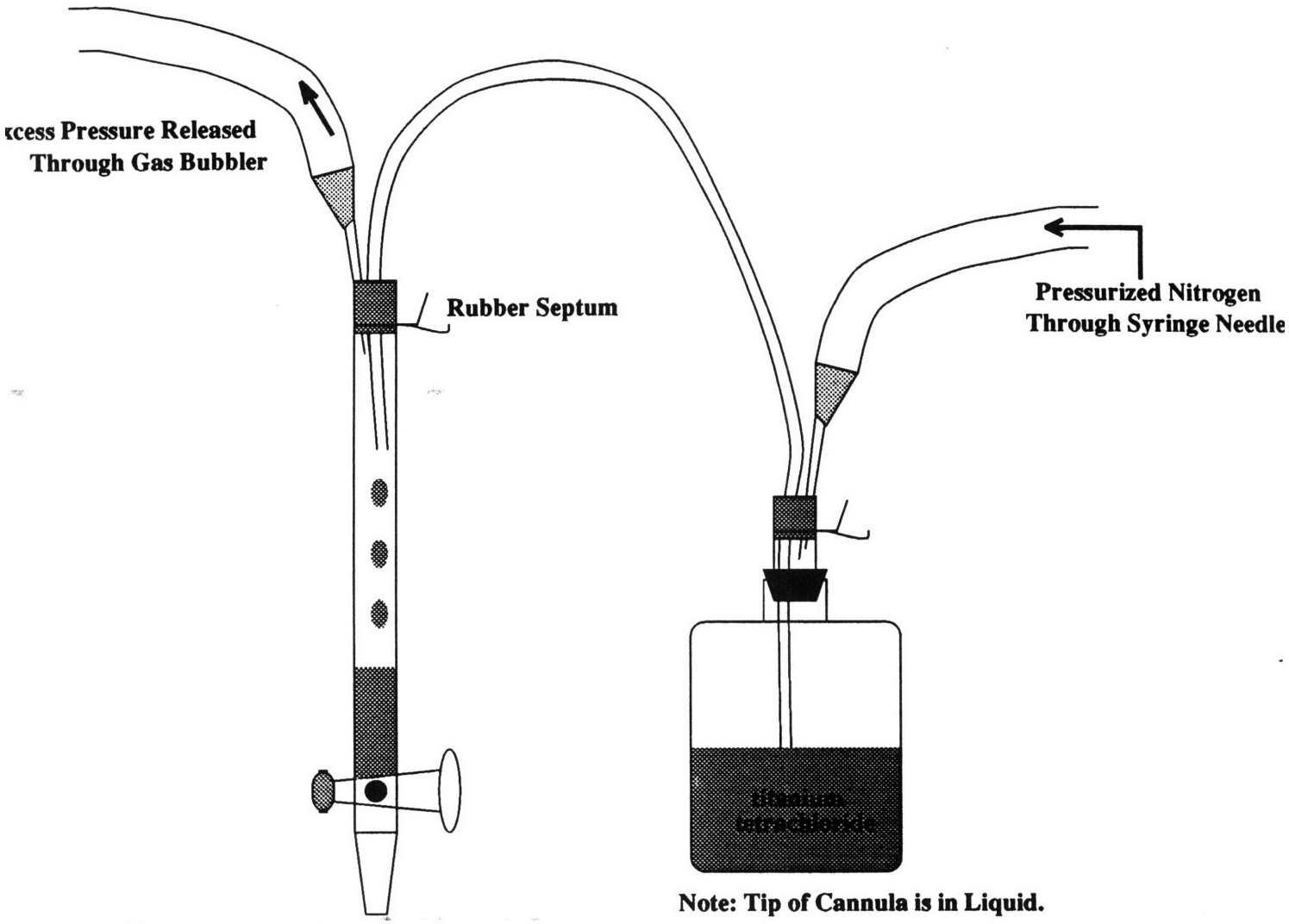

Figure 3-5: Configuration to Fill Buret with $TiCl_4$.

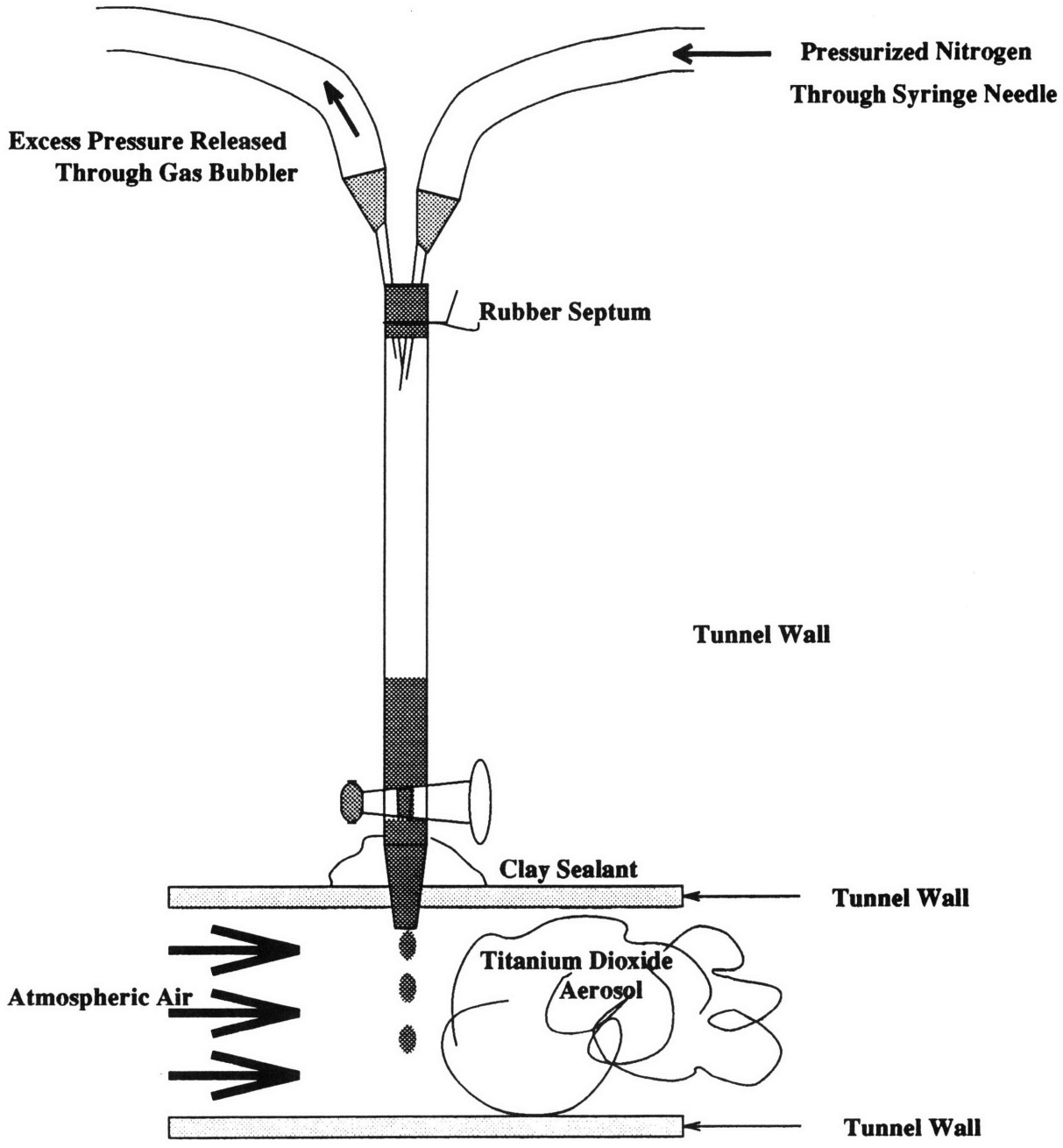

Figure 3-6: Configuration to Inject Aerosol into Wind Tunnel.

Maximum Accelerating Voltage	$200kV$
Maximum Magnification	330,000
Point-to-point Resolution	4.5 Å

Table 3.2: JEOL 200 TEM Specifications.

nient locations to adhere the grid flush with the channel wall. According to a data sheet provided by Ted Pella, Inc. [16], the thickness of the Formvar film alone ranged from 35 to $70nm$. The thickness of the copper rim of the grid was $\sim 15\mu m$ [16], below the estimated diffusive layer of $128\mu m$ in section A.1. However, estimated diffusive layers became as thin as the grid when the particle diameter approached $1\mu m$. This effect should be considered when analyzing the mass transfer.

A colloidal graphite water base paint, also from Ted Pella, Inc., adhered the grid to the channel wall. The tab was placed downstream of the grid to minimize disruption to the local flow field. Besides adhering the grid, a thin line of the paint was drawn to the side of the tunnel test section to a ground in order to conduct static electric charge off the grids. Once again this prevented deposition due to electric charge attraction. For reference, the average flake size according to Ted Pella [17] was $1\mu m$, much thinner than the estimated diffusive layer of $128\mu m$(see section A.1).

The TEM employed was a JEOL 200 (Japanese Electronics Corporation) maintained by the MIT Center of Material Science and Engineering. In table 3.2, significant specifications of the TEM are given[6].

For image analysis of the TEM photographs of deposition, two systems were used: *PC-Image* by Foster Findlay Associates coupled to a CCD camera and *Image 1.47* by the National Institute of Health coupled to a 16-gray level scanner. The first one was employed for the bulk of the data which were taken during the summer of 1992. I used the second system for the last set of data because of its easy use and easy access, i.e. cheaper access.

The first system read the photographs into the computer using a CCD camera. The camera was trained on the negatives which were placed on a light table to enhance contrast. Then the camera read created a digitial image for the computer. The *PC-*

Image program by Foster Findlay Associates ran on a DOS machine with Microsoft Windows. Unfortunately, the manual was poorly-written at best, and the setup cost $30/hour to use.

The second system was discovered after the bulk of the data were taken. *Image 1.47* published by the National Institute of Health was found installed in the Macintosh Computer Cluster at MIT. This program could also be copied to other Macintosh computers because it was in the public domain. It is easily obtained via anonymous file transfer protocol (ftp) from "zippy.nimh.nih.gov". An Apple Scanner using the accompanying software, Apple Scan version 1.0.2, was located in the CADLAB of the Martin Design Center, a part of the department of Mechanical Engineering at MIT.

The authors of *Image 1.47* recommended a Macintosh with 8MB memory or more to work with 3D images, 24-bit color or animation sequences. The program also required a monitor with the ability to display 256 colors or shades of gray. To take advantage of the 256 gray levels on the monitor a scanner with the ability to scan 256 shades of gray would be preferable. The main steps of the image analysis procedure were to obtain the most accurate representations of the deposition, i.e. the photos, and then count all the particles on the photo.

Chapter 4

Procedure

4.1 Obtaining a Deposition Sample

Prior to a test run, the top of the test section was removed to clean the inside tunnel walls of previous deposition and dirt with denatured alcohol. After cleaning, I affixed the TEM grids to the bottom tunnel wall taking care not to damage the grids and to keep them flush with the wall. The top was replaced, and a visual inspection of the entire apparatus ensured no aerosol escaped into the laboratory. Immediately before injection, the initial level of the buret was recorded, and a stopwatch was readied. Injection was then started by opening the stopcock on the buret while simultaneously starting the stopwatch. During each test run, I injected enough $TiCl_4$ to form approximately $10g$ of TiO_2(calculated from stoichiometry). The timer was stopped when smoke had been observed to cease exiting from the test section. Generally, this occurred in about fifteen minutes. Even though visible smoke may have ceased, I left the compressor on for an extra five minutes to ensure complete reaction of the $TiCl_4$.

4.2 TEM procedure

The TEM procedure gave us several photographs of the deposition on each grid. Starting and calibrating the electron microscope occupied the majority of the time; however, this part of the procedure partly determined the contrast of the images

obtained. After performing the startup procedure, I moved to the center of the grid at 20,000 magnification. Then I took five photographs of this area. After each photograph, I moved the grid in one direction until the microscope was trained on a new area of the grid. So, for each grid, I went to the approximate center of the grid, traversed the grid in one direction and took five different photographs. This averaged out any local deposition variations and avoided deposition abnormalities at the rim of the grid. After using the TEM, I unloaded the exposed negatives from the TEM and developed them. Contact prints were made from these negatives which were fed to an image analysis program to count and size particles.

4.3 Image Analysis

4.3.1 Scanning the Photos

To enable the computer to "see" my photos, I scanned them into a Macintosh computer using the Apple Scanner. The maximum resolution I used was 200 dots per inch (dpi) because scans at higher resolutions exceeded the memory capacity of the computers available. Most scans were 400-500 KB in size. The contrast and brightness levels of the graylevel scans were manipulated to obtain images which resolved the smallest particles noticeable to the naked eye on the photographs. Scans were saved in TIFF format because that was the recommended format for the image analysis program.

4.3.2 *Image 1.47*

The image analysis program enhanced the photographs, created black-and-white binary images, and measured the area of each particle. Enhancement was the most manual task and required interpretation of the photograph. Depending on how the photograph was enhanced, the continuum of gray was divided, and all pixels are switched to either black or white. With this binary image, the computer could easily measure the black particles on the white background.

Frequently, the particle's gray level matched the background's, so many particles had to be made darker or blacker against the gray background. This was accomplished by outlining the lighter particles with a mouse and then filling in the outlined particle with black. On the other hand, black objects determined not to be TiO_2 particles were erased, i.e. made white. To determine which particles needed to be accentuated, each scanned image was compared to the original photo which showed better contrast.

After all particles to be measured were converted to black particles, the image was thresholded. This meant that a gray level was chosen at which every pixel darker than this level was changed to black and every pixel lighter than this level was changed to white. The proper threshold level was when all the particles were black and everything else was white. With the proper level set, I created a binary which established the image as a simple black-and-white image.

To enable the computer to measure the particles with the real units of the photograph, the program had to have a length scale set. To do this, I drew a line between two points on the image. The corresponding distance on the photograph was then measured with a micrometer. The length of the line in pixels was assigned the real units from the micrometer. By setting the scale, the program could calculate the area of each in particle in square microns.

The final step for the program was to count and size each particle. The results were displayed in a separate window and from there saved on disk or sent to a printer. They were saved in tabular form on disk enabling retrieval using a spreadsheet program like *Excel* for further numerical analysis or by a text editor such as *TeachText* for obtaining just printouts.

The results were loaded into *Excel* because they were in the form of an area and needed further data handling. To convert to a diameter, I chose to calculate the diameter of the circle of equal area. Therefore, $d_p = \sqrt{(4/\pi)Area}$. Notice that d_p is the geometric diameter, not the aerodynamic diameter defined in Appendix A.4. Therefore, particle diameters tabulated in the results were the geometric diameters. The spreadsheet also sorted the particles by diameter which made counting easier.

4.3.3 *PC-Image*

The procedure for this program was very similar to that of *Image 1.47*. The major difference was that contact prints of the negatives were unnecessary. This was due to the CCD-camera and the light table which read the negative. However, further analysis which was done on *Excel* in the previous case had to be done manually.

Chapter 5

Results

5.1 Summer 1992

Preliminary measurements were taken in the summer of 1992 to complete the grant proposal to NIH. The work done during this period was performed by Kurt Roth and myself. Our results also did not vary significantly from test to test demonstrating repeatability of our experimental methods. They also showed that there was greatly enhanced deposition in secondary flow. There were two minor faults, though. An expansion section before the test section caused the flow to stall, and our control over the injection was less than satisfactory. A test was also run without any aerosol injection to measure background noise.

5.1.1 No Step

259 particles of all sizes deposited at this location. The total number of particles that deposited here was much lower than at the other locations. The particle size distribution had its peak from .15 to .35μm. Around this peak, particles less than .15μm deposited more than particles greater than .15μm. The deposition rapidly vanished when approaching $d_p = 1\mu m$.

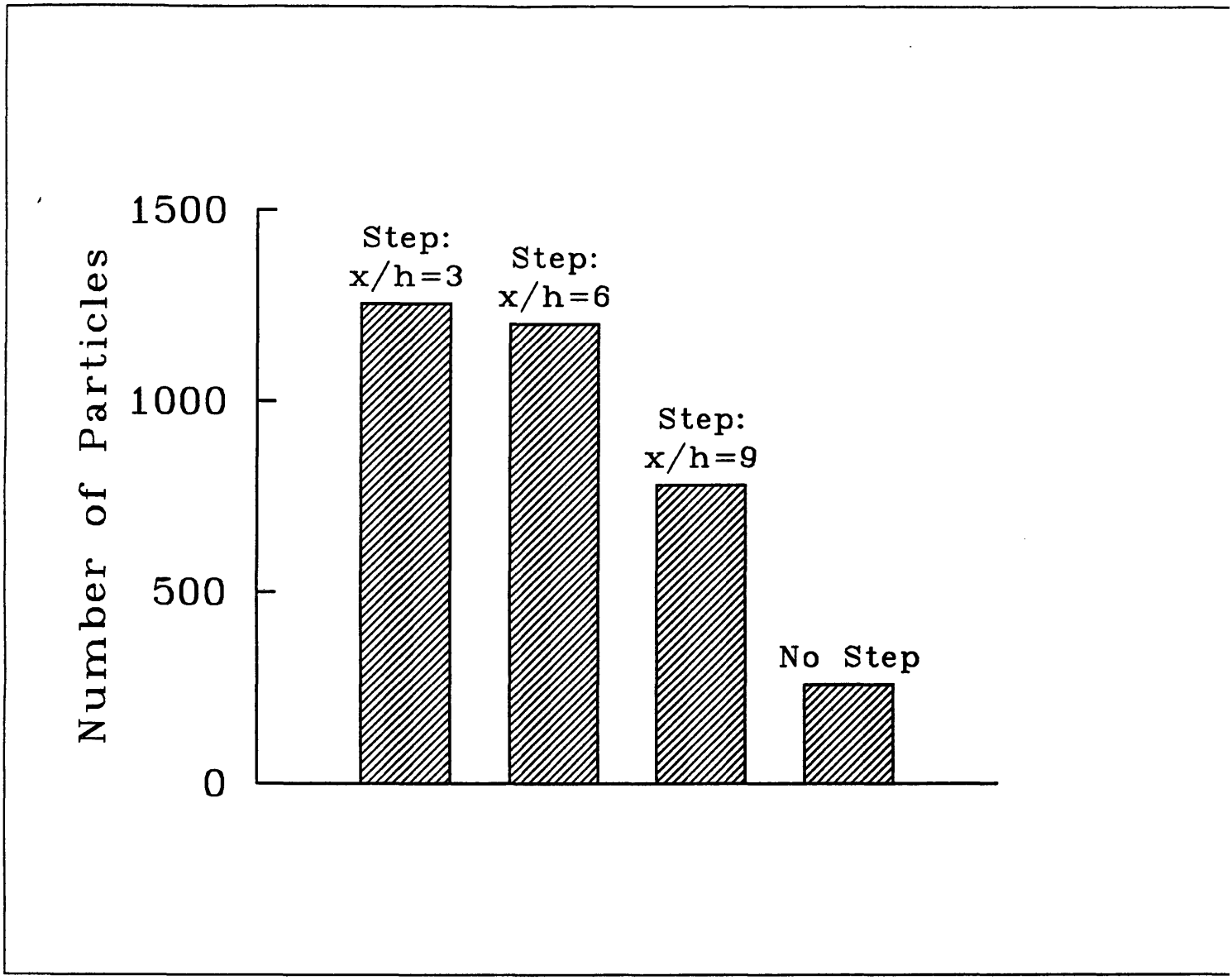

Figure 5-1: Total Deposition Count- Summer 1992 (Kurt Roth & Michael Feng).

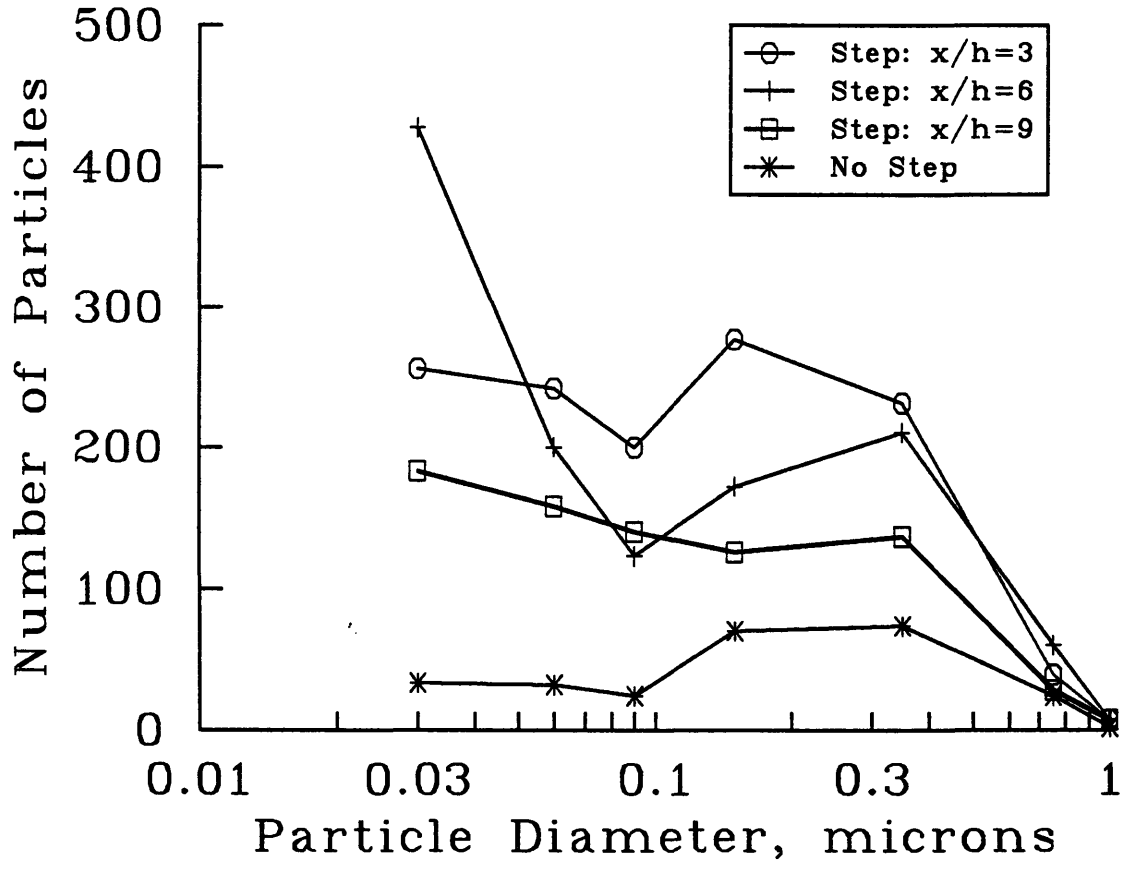

Figure 5-2: Size Distribution of Deposited Aerosol at Several Locations- Summer 1992 (Kurt Roth & Michael Feng).

5.1.2 x/h = 3

This location contained the highest total number of particles deposited. 1254 particles of all sizes deposited here. This deposition count was almost five times greater than for the case with no step. The particle size bin with the largest number of particles was from .02 to .04μm. There was a steady drop in deposition with increasing particle diameter until d_p reached about .35μm. At this particle diameter there was a slight increase in deposition. The deposition of particles with diameters larger than .35μm rapidly vanished after this.

5.1.3 x/h = 6

The number of particles regardless of diameter deposited was 1201. This result was only four percent off of the total deposition for x/h = 3. The particle size bin with the largest number of particles was from .02 to .04μm. This location showed a minor peak, too. In this case it was around .15 to .35μm in diameter. At particle diameters greater than at the peak, deposition vanished.

5.1.4 x/h = 9

The total number of particles dropped significantly from the x/h = 6 case. 780 particles of all sizes landed at this location. This was only 62 percent of the x/h = 3 case. Particles from .02 to .04μm again comprised the majority of the particles, in this case 183 out of 780. There was also the steady decline to d_p = .35μm when there was a sudden surge in deposition and then a rapid decline in deposition with increasing particle diameter.

5.1.5 Background Noise

A test run was performed to determine the background noise of our deposition measurements. This was done by simply turning on the compressor, and allowing normal laboratory air to pass through the test section with grids mounted inside. Upon examination of the grids, no dust particles could be found, so it was concluded that the

background noise was effectively zero.

5.2 Spring 1993

The purpose of running this test was to test some solutions to the problems encountered during the summer of the previous year. The expander was elongated to prevent stall of the flow, and the injection system documented in the apparatus section was used to overcome the unreliability and uncertainties of the previous system.

5.2.1 No Step

This case contained the most particles regardless of particle diameter, 430. It had its peak at the lowest particle diameter bin which was from .03 to .04μm. This, too, exhibited a minor peak at particle diameters between .1 and .2μm.

5.2.2 x/h = 3

Within the secondary flow, this position had the highest total number of particles deposited which was 240 particles. Particles between .01 and .04μm constituted the majority of the total deposition at this location. The minor peak occurred in the .20 to .25μm particle diameter bin.

5.2.3 x/h = 6

A significant drop from the x/h = 3 case happened in the total number of particles deposited. Only 154 particles deposited at this location, a 35 percent reduction. Particles with diameters between .03 and .04μm occupied the majority of the deposition. Again, a minor peak or increase in deposition with increasing particle diameter occurred when d_p = .3 to .4μm.

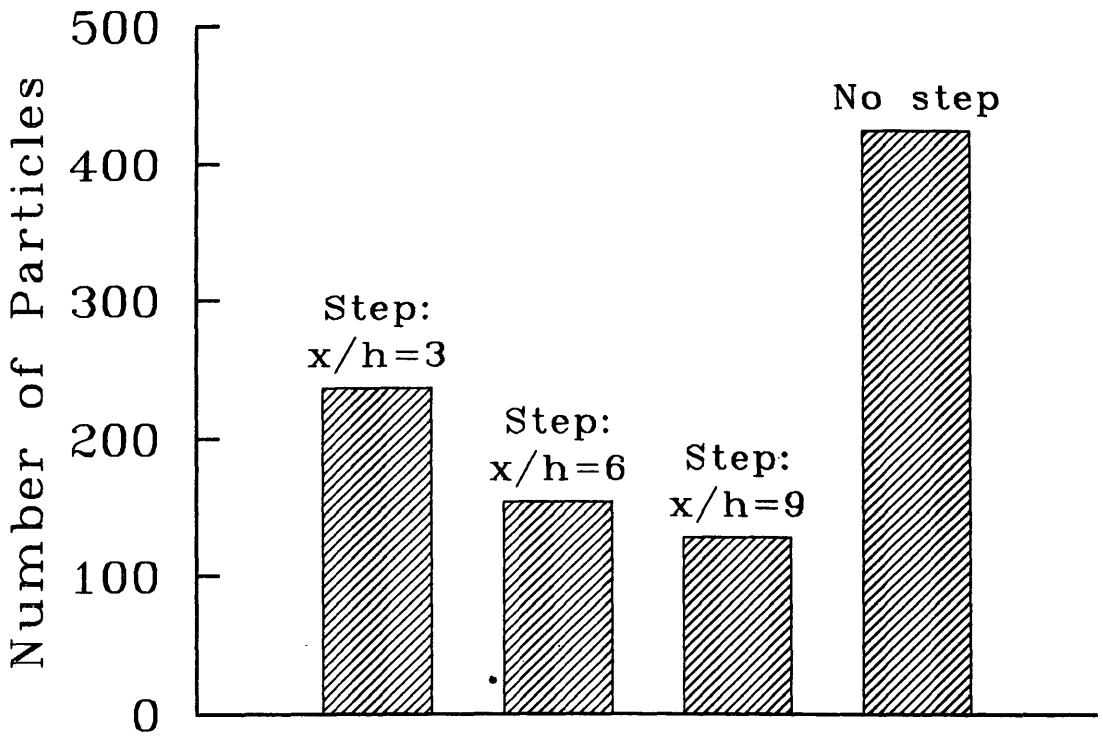

Figure 5-3: Total Deposition Count- Spring 1993.

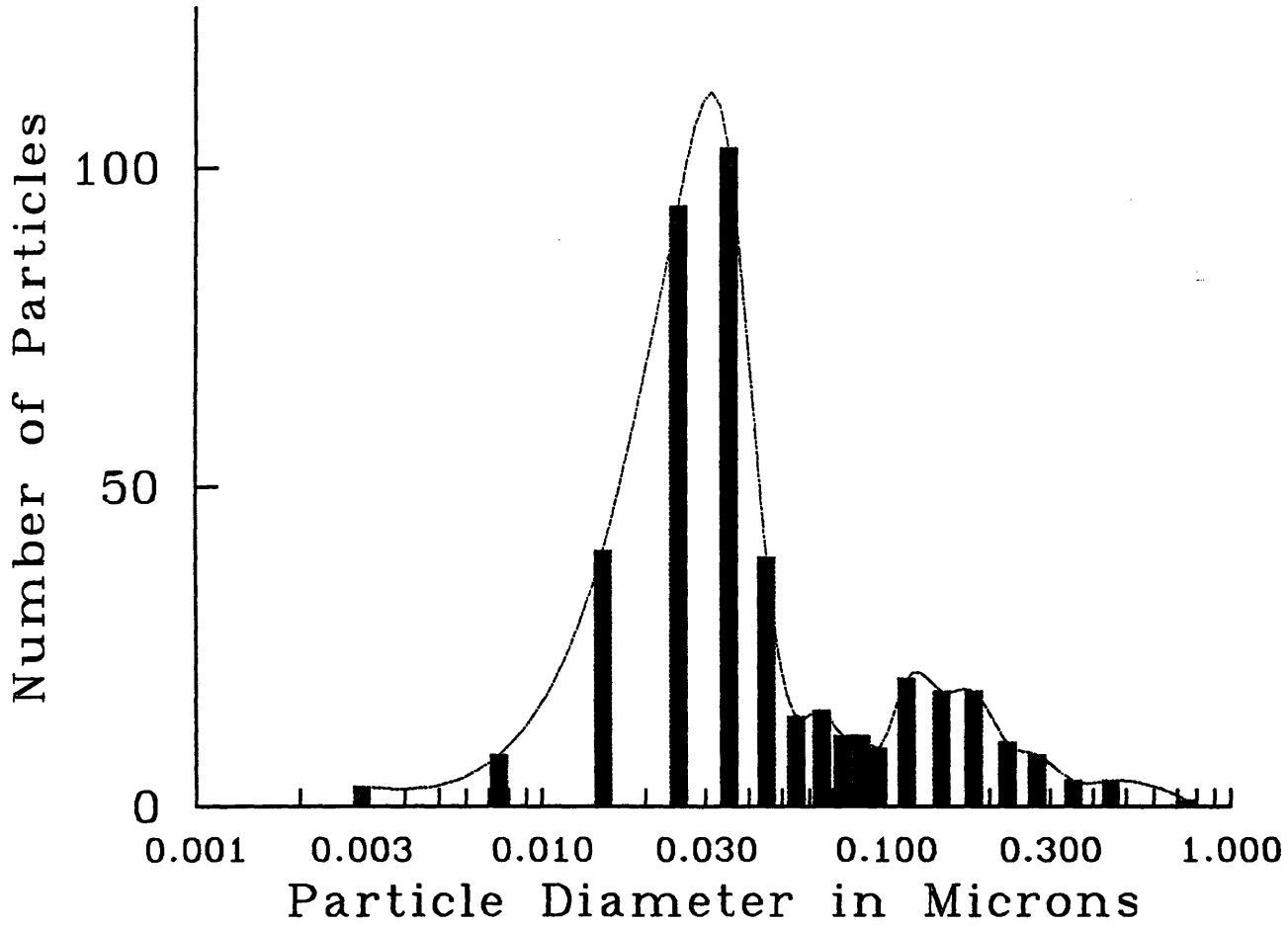

Figure 5-4: Size Distribution (no step)- Spring 1993.

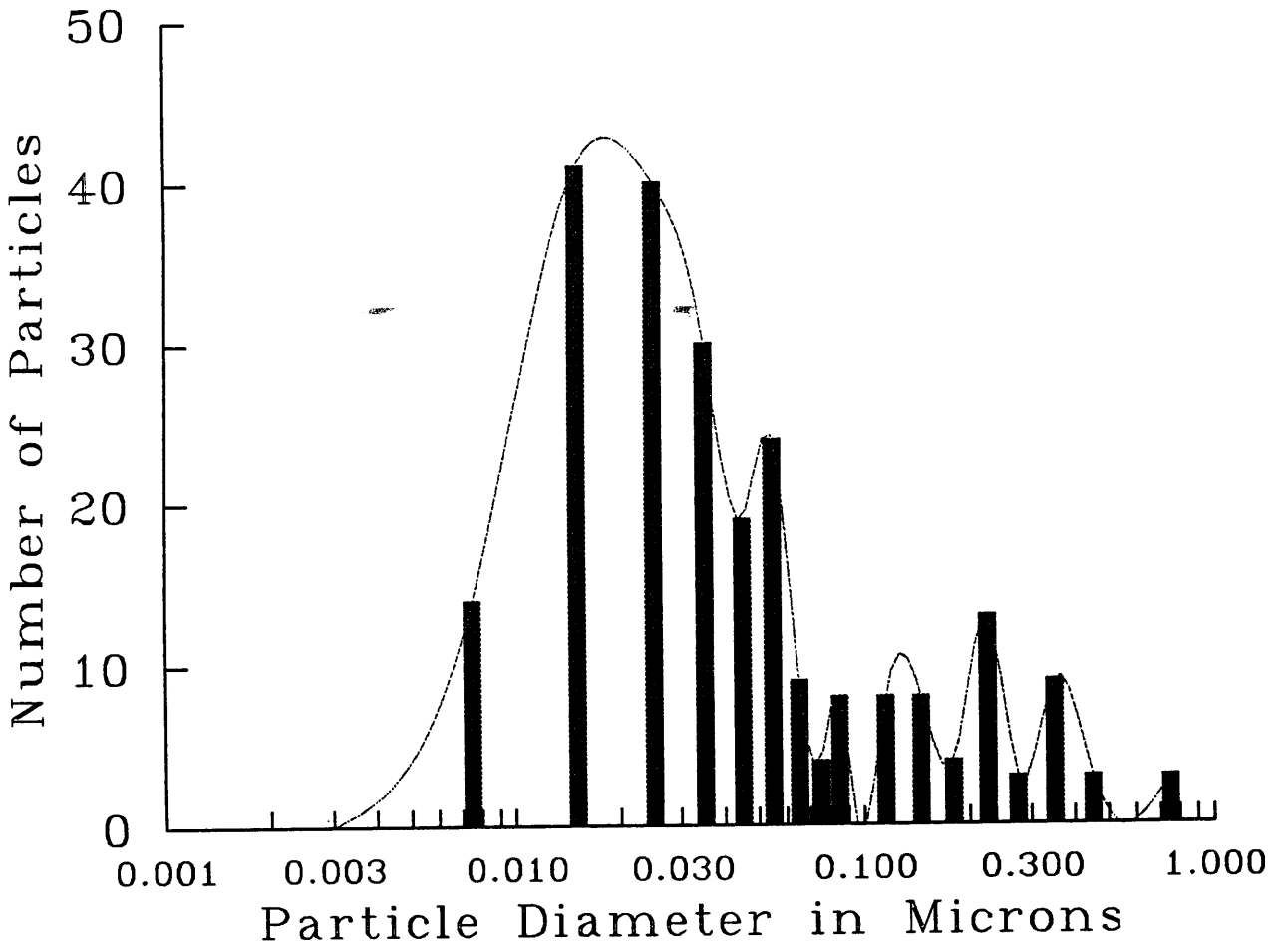

Figure 5-5: Size Distribution (x/h=3)- Spring 1993.

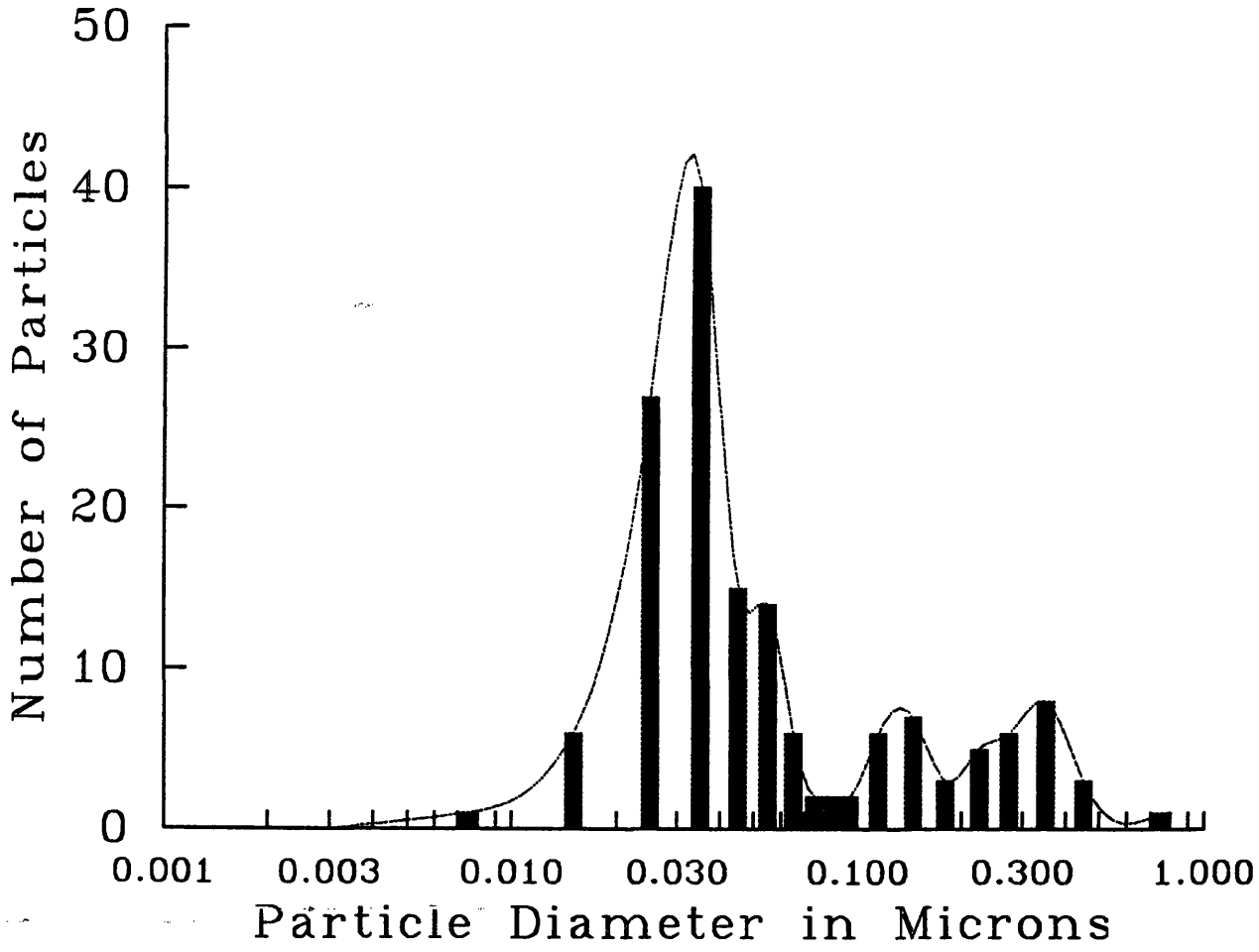

Figure 5-6: Size Distribution (x/h=6)- Spring 1993.

5.2.4 x/h = 9

127 particles in total deposited in this case. This was only a 17 percent reduction from the x/h = 6 case. Particles in the diameter bins of .04 to .05μm and .05 to .06μm made up the majority of the deposition. The minor peak occurred shortly after at $d_p \simeq .1\mu m$.

It should also be noted that large amounts of foreign particulates deposited on this grid. Particles were determined as foreign by a square or rectangular shape with a length $\sim 1nm$. These foreign particles also landed on other grids but not nearly to the extent that they did in this case.

5.3 Comparison Between 1992 and 1993

There were several striking differences between the measurements made during the summer of 1992 and those done during the spring of 1993. Very few particles on the order of one micron were detected in the latter test. On the contrary many more small particles were detected in 1993 than in 1992. One very disturbing result is that there were twice as many particles for the case with no step than any of the cases with a step upstream in 1993.

However, the shapes of the total deposition curves between 1992 and 1993 were similar for the cases behind the step. A trend for a major peak in deposition followed by a minor peak in deposition with increasing particle diameter was also shared between the two bodies of tests.

Both injector systems also deposited aerosol right beneath the injection port. This was very obvious because a visible mound of TiO_2 grew underneath the hose or buret. These particles must have been larger particles that deposited by gravitational force. Some aerosol also deposited via inertial impaction when the flow was compressed before the test section. Again this deposition was highly visible.

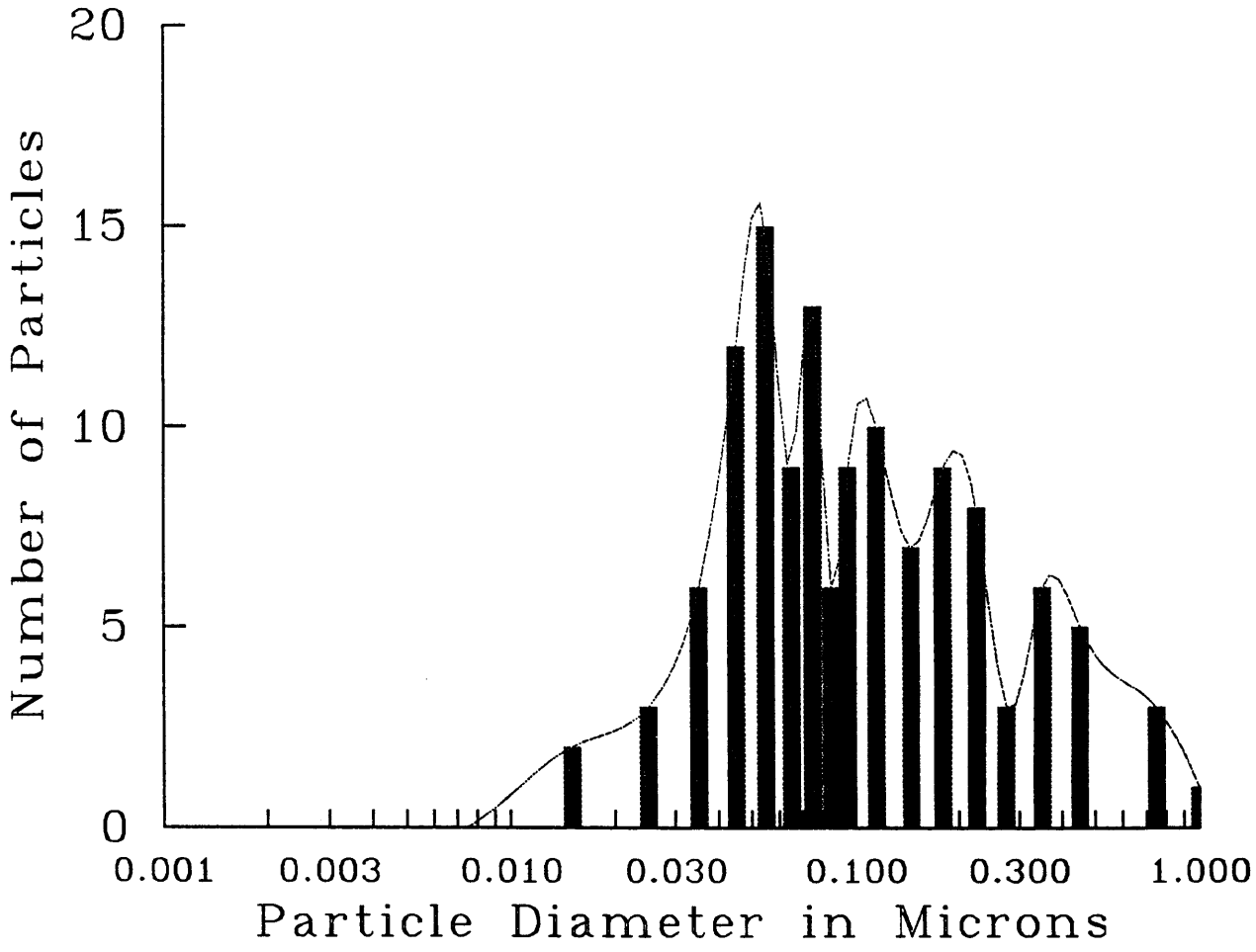

Figure 5-7: Size Distribution (x/h=9)- Spring 1993.

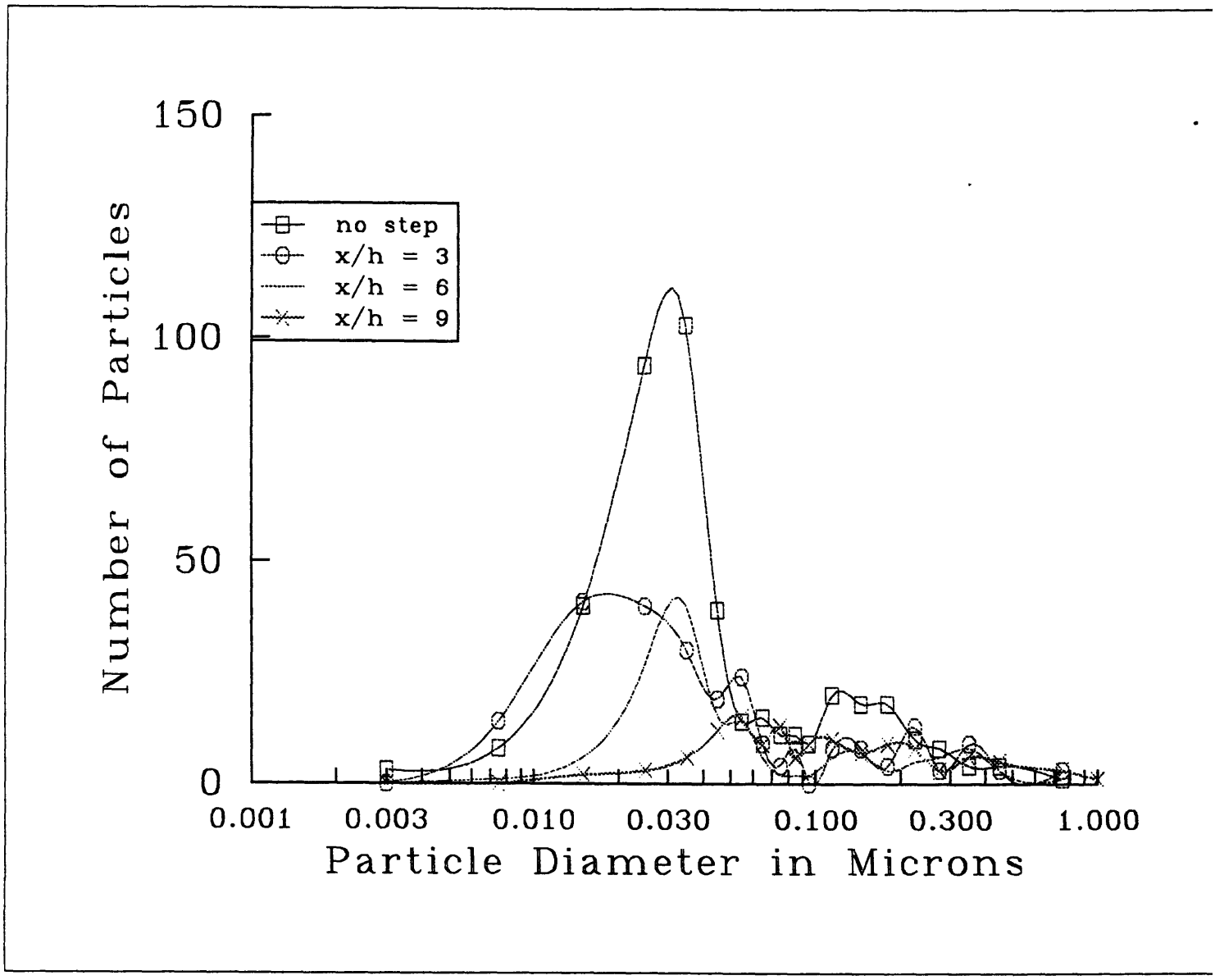

Figure 5-8: Size Distribution (All Cases)- Spring 1993.

Range of d_p $[\mu m]$	d_p in calculation	Schmidt Number Sc	Stokes Number Stk	δ $[\mu m]$
.02-.04	.03	2261	3.10e-06	56.38
.05-.07	.06	8021	1.24e-05	41.08
.08-.10	.09	16196	2.79e-05	34.46
.11-2.0	.15	37266	7.76e-05	27.98
.21-.50	.35	127322	4.22e-04	20.58
.50-1.00	.75	317734	1.94e-03	16.38
1.00+	1.0	420046	3.45e-03	15.27

Table 5.1: Theoretically Determined Parameters of Deposition- Summer 1992.

5.4 The Influence of Secondary Flows on Deposition

5.5 Uncertainty Analysis

To obtain an estimate of the uncertainty, a Gaussian distribution was assumed for each particle range; however, a Poisson distribution possibly was more appropriate. For each particle range and grid location, the average number of particles detected was calculated. Using Student's T distribution, an interval that contained the true mean with a confidence of 95 percent was calculated. The uncertainty analysis was performed solely on the data from the spring of 1993. Judging from experience with the injection system, uncertainty for the 1992 data will be high.

Range of d_p $[\mu m]$	d_p in calculation	Schmidt Number Sc	Stokes Number Stk	δ $[\mu m]$
.001-.005	.003	24.54	2.23e-08	232.35
.005-.010	.0075	156	1.39e-07	147.73
.010-.020	.015	604	5.57e-07	105.37
.020-.030	.025	1605	1.55e-06	82.53
.030-.040	.035	3014	3.03e-06	70.49
.040-.050	.045	4783	5.01e-06	62.81
.050-.060	.055	6870	7.49e-06	57.37
.060-.070	.065	9238	1.05e-05	53.28
.070-.080	.075	11856	1.39e-05	50.06
.080-.090	.085	14699	1.79e-05	47.44
.090-.100	.095	17742	2.23e-05	45.26
.100-.130	.115	24350	3.27e-05	41.81
.130-.160	.145	35332	5.21e-05	38.10
.160-.200	.180	49377	8.02e-05	35.04
.200-.250	.225	68819	1.25e-04	32.25
.250-.300	.275	91651	1.87e-04	30.02
.300-.400	.350	127321	3.03e-04	27.65
.400-.500	.450	175993	5.01e-04	25.50
.500-1.000	.750	317734	1.39e-03	22.00

Table 5.2: Theoretically Determined Parameters of Deposition- Spring 1993.

Range of d_p $[\mu m]$	Ratio for x/h = 3	Ratio for x/h = 6	Ratio for x/h = 9
.02-.04	7.76	13.0	5.55
.05-.07	7.56	6.25	4.94
.08-.10	8.33	5.13	5.83
.11-2.0	3.96	2.46	1.80
.21-.50	3.14	2.85	1.85
.50-1.00	1.63	2.5	1.17
1.00+	3.5	3.5	3.5

Table 5.3: $g_m/g_{m_{no\ step}}$: Ratio of Mass Transfer Coefficients- Summer 1992.

Range of d_p $[\mu m]$	Ratio for x/h = 3	Ratio for x/h = 6	Ratio for x/h = 9
.001-.005	0	0	0
.005-.010	1.75	.125	0
.010-.020	1.03	.15	.05
.020-.030	.426	.287	.032
.030-.040	.291	.388	.0583
.040-.050	.487	.385	.308
.050-.060	1.71	1	1.07
.060-.070	0.6	0.4	0.6
.070-.080	.364	.182	1.18
.080-.090	.727	.182	.545
.090-.100	0	.222	1
.100-.130	0.4	0.3	0.5
.130-.160	.444	.389	.389
.160-.200	.222	.167	0.5
.200-.250	1.3	0.5	0.8
.250-.300	.375	.75	.375
.300-.400	2.25	2	1.5
.400-.500	0.75	0.75	1.25
.500-1.000	3	1	4

Table 5.4: $g_m/g_{m_{no\ step}}$: Ratio of Mass Transfer Coefficients- Spring 1993.

Range of d_p $[\mu m]$	no step	x/h = 3	x/h = 6	x/h = 9
.001-.005	$.5 \pm 1.591$	0 ± 0	0 ± 0	0 ± 0
.005-.010	1.5 ± 2.756	2.75 ± 6.671	0.2 ± 0.555	0 ± 0
.010-.020	8 ± 1.837	8.25 ± 4.184	1.2 ± 2.040	0.4 ± 1.110
.020-.030	18.5 ± 14.319	8 ± 4.108	5.4 ± 5.012	0.6 ± 1.666
.030-.040	20.5 ± 22.065	6 ± 6.750	8 ± 4.888	1.2 ± 2.691
.040-.050	7.75 ± 5.257	3.75 ± 2.717	3 ± 2.483	2.4 ± 3.577
.050-.060	2.75 ± 2.717	4.75 ± 4.184	2.8 ± 2.040	3 ± 4.210
.060-.070	3 ± 5.257	$1.75 \pm .795$	1.2 ± 1.360	1.8 ± 2.691
.070-.080	2.25 ± 2.717	$0.75 \pm .795$	$0.4 \pm .680$	2.6 ± 1.883
.080-.090	2.25 ± 3.528	1.5 ± 2.054	$0.4 \pm .680$	$1.2 \pm .555$
.090-.100	1.75 ± 3.759	0 ± 0	$0.4 \pm .680$	1.8 ± 1.039
.100-.130	4 ± 5.662	1.5 ± 2.054	1.2 ± 1.619	$2 \pm .878$
.130-.160	3.5 ± 2.756	$1.5 \pm .919$	$1.4 \pm .666$	1.4 ± 1.415
.160-.200	3.5 ± 3.787	0.75 ± 2.386	$0.6 \pm .680$	1.8 ± 1.360
.200-.250	2 ± 1.299	$2.5 \pm .919$	1 ± 1.241	$1.6 \pm .680$
.250-.300	1.5 ± 1.299	$0.5 \pm .919$	$1.2 \pm .555$	0.6 ± 1.110
.300-.400	0.75 ± 1.523	$1.75 \pm .795$	$1.6 \pm .680$	1.2 ± 1.360
.400-.500	0.75 ± 1.523	$0.5 \pm .919$	0.6 ± 1.110	1 ± 1.241
.500-1.000	$0.25 \pm .795$	$0.5 \pm .919$	$0.2 \pm .555$	$0.6 \pm .680$

Table 5.5: 95 % Confidence Interval for the Mean Number Expected in Each Particle Range.

Chapter 6

Discussion

6.1 Conclusion

From the data taken in 1992, the effect of secondary flows on deposition was substantial. The mass transfer coefficient could be raised almost thirteen times that of the no step case when x/h = 6 and $0.2 < d_p < 0.4\mu m$. The other mass transfer coefficients were all equal to or greater than the corresponding case with no step. The total number of particles deposited was almost five times greater for x/h = 3 than for the no step case. The deposition mechanisms present in secondary flows definitely enhanced the deposition, particularly that of the ultrafine aerosols.

The enhancement in deposition became greater as the particle diameter shrank. All cases behind the step had their peak deposition at the lowest particle diameter measured. Therefore, the deposition mechanisms present in secondary flows affected ultrafine aerosols significantly. The particles were probably driven closer to the wall by the vortex causing a higher concentration gradient to drive mass transfer.

There were two possible explanations for the deposition being higher at x/h = 6 than at x/h = 3. First, the flow field at x/h = 3 was hypothesized to be where the main vortex joined the corner vortex as described by Faramarzi and Logan(see Figure 2-3). Here the flow encounters a sharp change in direction creating inertial compounding effects on the diffusive deposition. The other theory was that if the x/h = 3 location was still within the main vortex then there would be more time for the

aerosol to diffuse to the wall.

The theory that inertia enhanced the deposition of was borne out by the two sets of data. At the reattachment point, x/h = 9, small particles did not deposit as highly as before the reattachment point. The diffusive boundary layer is still quite large due to the separation of the flow, so the mass transfer is lower.

Frequently, there was a minor peak in the particle size distributions after the major peak in deposition. These could be due to the particle size distribution of the bulk concentration. In other words, if there were more particles of a certain particle size then the likelihood of encountering them in deposition photographs is higher. The deposition mechanisms present in the secondary flows might also have a lesser effect on the particle sizes between the peaks. For example, the particle sizes that did not deposit in large amounts might have been too large for Brownian diffusion to act and too small for inertia to impact them against the wall.

The mass transfer coefficients determined from the 1993 data was not very reliable because of the small size of the sample. More questions arose when examining the data. Nearly twice as many particles landed at the location before the step than at any location behind the step. Consequently, many mass transfer coefficient ratios were less than unity. Obviously, more tests should be run to see if this new phenomena remains. If these measurements were valid, then the mass transfer coefficients are actually lower in the secondary flow than before the step.

If the deposition was lower in the secondary flow than upstream then the separation of the diffusive boundary layer from the wall could be important. The flow field and aerosol seeding was more uniform and controlled in 1993 than in 1992. So, these results might be more valid than those obtained in 1992.

However, the shape of the total deposition curve for the cases behind the step was similar to that of 1992. With regards to the deposition within the secondary flow, much of the same phenomena from the 1992 data occurred. The minor peak following the major peak in the particle size distribution also could be found in the 1993 data.

The procedure developed was successful in creating and measuring the deposition of ultrafine aerosol The TEM photos verified that the particles were "ultrafine". These

photos also provided excellent spatial resolution and highly localized measurements compared to other aerosol measurement techniques. The image analysis procedure counted and sized particles in a highly automated fashion. The major drawback to the system was the price in time and equipment.

6.2 Errors

6.2.1 Foreign Particles

The source of the foreign particulates detected in 1993 remains a mystery. They appear to be of a crystalline structure with a low density. However, there are a few plausible hypotheses. The ambient air might have been contaminated by other experiments taking place in the laboratory. Black RTV also might have entered the flow since the HCl in the buret corroded RTV that coated the rubber septum. This RTV jammed the buret, so RTV might have come out of the buret.

Sometimes distinguishing between the foreign particles and actual TiO_2 particles became difficult. This could have drastically affected the particle counts I got for the x/h = 9 case. The error would be that too few smaller particles were counted.

6.2.2 Variance in Particle Size Distributions

There were two changes in the apparatus which were the likely causes of variance in the particle size distributions. The humidity was probably much lower in 1993 than in 1992. The test run in 1993 was on March 31st, still part of the cold winter that occurred in Boston. On the other hand, the measurements from 1992 were done during the middle of summer when the humidity level is usually high. Less humidity implies less than a complete reaction between the $TiCl_4$ and the water vapour of air. Unfortunately, no measurements of the humidity level were taken. There was also the expansion that had stall. Visible deposition on the sides occurred presumably due to the secondary flow induced the separation of the flow from the sides. If there was a tendency for this secondary flow to deposit ultrafine aerosols then

the bulk concentration entering the test section would contain less ultrafine aerosols. The variance in the particle size distributions most likely came from changes in the apparatus.

6.2.3 Illegitimate Errors

Non-flush Grids

The airstream might have blown the grids off of its flush mounting against the tunnel. This could have created abnormal flow fields around the grids affecting deposition. On one occasion, a grid drastically moved away from the wall with a visible white ring of TiO_2 around the grid. This test was not used in the final results.

Marred Photographs

During the development process, several negatives were marred rendering them useless. This problem entailed normalization of particle counts which caused uncertainty in the results.

Injection System of 1992

This injection system had a very high uncertainty in the total amount of $TiCl_4$ injected. Measuring this quantity consisted of watching the liquid flow from one point to another in the hose and timing it. Then the distance was divided by the time to obtain a velocity. This method assumed a constant velocity which was not always true and a constant cross-sectional area of the hose. The velocity did not remain constant because as the TiO_2 clogged the end of the tube the velocity decreased. The high uncertainties in total mass injected amplified the uncertainties in particle counts that had to be normalized to a specified total mass injection.

6.3 Recommendations for Procedure

Tighter control of the testing conditions needs to be exercised. The noticeable differences between the results of 1992 and 1993 demonstrate a need to ameliorate changes in the atmospheric air. A clean room which has a specified amount of particulates in the air is highly desirable in maintaining low background noise in measurements. Humidifying the air ensures as complete a reaction as possible. Keeping the humidity level constant at least will be beneficial.

To eliminate one of the degrees of freedom, switch to a monodisperse aerosol. Then all particles can be assumed to be the same. Monodisperse aerosol generators are available on the market. A monodisperse aerosol can also be generated by filtering a polydisperse aerosol. This method will inevitably have other particle sizes, but most of the particles should be the same.

Tests should also be run at different locations. Running a test at $x/h = 12$ or 15 can elucidate the deposition occurring after reattachment. Running a test with three or more grids at the same distance along the length of the test section will check for any deposition bias along the width of the test section. A test should also have been run with no aerosol injected to test for background noise again.

To measure actual mass transfer coefficients, measuring the bulk concentration is necessary. To this end, a particle counter should be obtained. A constant bulk concentration is also necessary since real-time measurements with the TEM are impossible. A constant bulk concentration might be obtained by building a settling section where the aerosol can be mixed to the right concentration before injection.

The image analysis program, *Image 1.47*, recommends grayscale pictures with 256 levels of gray. Therefore, a 256 gray level scanner should be used to scan the photos rather than the 16 gray level scanner employed in this thesis. Because 256 gray level scans occupy much more computer memory, powerful computers with large internal memories should be used, e.g. a Quadra. Powerful computers help process large quantities of data faster, too.

6.4 Recommendations for Further Study

Once the aforementioned difficulties have been solved, development of the model of ultrafine aerosol behaviour in the lung will continue. It has been proposed to build a wedge in the flow to simulate a bifurcation or bend the channel to simulate curved flows. The ultrafine aerosol technique developed here can be employed in many other situations such as deposition due to thermophoresis or deposition in laminar flow.

Appendix A

Calculations

A.1 Estimate of Diffusive Boundary Layer

An estimate for the diffusive boundary layer was done using equation 2.6. First, I calculated $\mathcal{D}$ to find the Schmidt number, Sc.

1. $\mathcal{D} = C\frac{k_B T}{\mu_{air} 3\pi d_p}$

   where k_B is Boltzmann's constant.

2. $\mathcal{D} = 24.3[\frac{(1.3805\times10^{-23}J/K)(293K)}{(1.83\times10^{-5}kg/m-s)3\pi(.01\times10^{-6}m)}]$

3. $\mathcal{D} = 5.70 \times 10^{-8} m^2/s$

   Assuming Re_{d_h} is 3568 and plugging into equation 2.6, $\delta = 28.5\frac{(0.02345m)(5.7\times10^{-8})^{\frac{1}{3}}}{(3548)^{\frac{7}{8}}(\frac{1.83\times10^{-5}}{1.183})^{\frac{1}{4}}}$.
   After algebra $\Longrightarrow \delta = 128\mu m$.

A.2 Calculation of Stokes Number

Stokes number, Stk, is equal to τ/tau_{flow}.

$$\tau = \frac{\rho_p d_p^2}{18\mu_{air}} \tag{A.1}$$

$$\tau_{flow} \simeq \tau_{Kolmogorov} \tag{A.2}$$

Equation A.2 only applies for the mean turbulence of the channel flow, not for any secondary flows. The following derivation of $\tau_{Kolmogorov}$ was done by Colmenares[2]:

1. $\sqrt{\frac{\nu}{\epsilon}}$
2. $\varepsilon \cong \frac{4}{d_h} U^3 (f/8)^{3/2}$
3. $\cong \frac{4}{d_h} U^3 (0.316/8)^{\frac{3}{2}} (Re_{d_h}^{-1/4})^{3/2}$
4. $= 0.0314 \frac{U^3}{d_h} Re_{d_h}^{\frac{3}{8}}$
5. $\tau_f = (0.0314)^{-1/2} (\frac{d_h \nu}{U^3})^{1/2} Re_{d_h}^{3/16}$
6. $\tau_f = 5.64 (\frac{d_h}{U}) Re_{d_h}^{-5/16}$

A.3 Hydraulic Diameter

- height of channel = 6 inches
- width of channel = 1/2 inch

1. $d_h \equiv \frac{4 \times cross-sectional\ area}{wetted\ perimeter} = \frac{4hw}{2(h+w)}$
2. $d_h = \frac{4(6)(1/2)}{2(6+1/2)}$
3. $d_h = 12/13$ inches
4. $d_h = .0234m$

$\Longrightarrow D_h = .0234m.$

A.4 Aerodynamic Diameter Conversion

According to Hinds[8]:

$$\frac{\rho_p d_p^2 g}{18\mu} = \frac{\rho_o d_{aerodynamic}^2 g}{18\mu} \tag{A.3}$$

where ρ_o is unit density, ie. $1g/cm^3$. Solving for d_p, we get $d_p = \sqrt{\frac{1.0}{4.17}(1\mu m)^2}$ where $4.17g/cm^3$ is the density of TiO_2. So, $d_p \simeq .49\mu m$, or the actual diameter equals 49 percent of the aerodynamic diameter.

$\Longrightarrow d_{geometric} = d_p \simeq .49(d_{aerodynamic})$.

A.5 Uncertainty Calculations

The average and standard were calculated for each particle size range. From the number of photographs taken and the desired 95 % confidence level, the t-statistic was looked up in a table.

				No step				x/h = 3	
Bin Range	Avg	Standard Dev	t-stat	Bound	Avg	Standard Dev	t-stat	Bound	
0.001	0.5	1	3.182	1.591	0	0	3.182	0.000	
0.005	1.5	1.7320508	3.182	2.756	2.75	4.1932485	3.182	6.671	
0.01	8	1.1547005	3.182	1.837	8.25	2.6299556	3.182	4.184	
0.02	18.5	9	3.182	14.319	8	2.5819889	3.182	4.108	
0.03	20.5	13.868429	3.182	22.065	6	4.2426407	3.182	6.750	
0.04	7.75	3.3040379	3.182	5.257	3.75	1.7078251	3.182	2.717	
0.05	2.75	1.7078251	3.182	2.717	4.75	2.6299556	3.182	4.184	
0.06	3	2.7080128	3.182	4.308	1.75	0.5	3.182	0.795	
0.07	2.25	1.7078251	3.182	2.717	0.75	0.5	3.182	0.795	
0.08	2.25	2.2173558	3.182	3.528	1.5	1.2909944	3.182	2.054	
0.09	1.75	2.3629078	3.182	3.759	0	0	3.182	0.000	
0.1	4	3.5590261	3.182	5.662	1.5	1.2909944	3.182	2.054	
0.13	3.5	1.7320508	3.182	2.756	1.5	0.57735027	3.182	0.919	
0.16	3.5	2.3804761	3.182	3.787	0.75	1.5	3.182	2.386	
0.2	2	0.81649658	3.182	1.299	2.5	0.57735027	3.182	0.919	
0.25	1.5	1.9148542	3.182	3.047	0.5	0.57735027	3.182	0.919	
0.3	0.75	0.95742711	3.182	1.523	1.75	0.5	3.182	0.795	
0.4	0.75	0.95742711	3.182	1.523	0.5	0.57735027	3.182	0.919	
0.5	0.25	0.5	3.182	0.795	0.5	0.57735027	3.182	0.919	
95%	Confidence	Level							
				x/h = 6					x/h = 9
Bin Range	Avg	Standard Dev	t-stat	Bound		Avg	Standard Dev	t-stat	Bound
0.001	0	0	2.776	0.000		0	0	2.776	0.000
0.005	0.2	0.4472136	2.776	0.555		0	0	2.776	0.000
0.01	1.2	1.6431677	2.776	2.040		0.4	0.89442719	2.776	1.110
0.02	5.4	4.0373258	2.776	5.012		0.6	1.3416408	2.776	1.666
0.03	8	3.9370039	2.776	4.888		1.2	2.1679483	2.776	2.691
0.04	3	2	2.776	2.483		2.4	2.8809721	2.776	3.577
0.05	2.8	1.6431677	2.776	2.040		3	3.391165	2.776	4.210
0.06	1.2	1.0954451	2.776	1.360		1.8	2.1679483	2.776	2.691
0.07	0.4	0.54772256	2.776	0.680		2.6	1.5165751	2.776	1.883
0.08	0.4	0.54772256	2.776	0.680		1.2	0.4472136	2.776	0.555
0.09	0.4	0.54772256	2.776	0.680		1.8	0.83666003	2.776	1.039
0.1	1.2	1.3038405	2.776	1.619		2	0.70710678	2.776	0.878
0.13	1.4	1.3416408	2.776	1.666		1.4	1.1401754	2.776	1.415
0.16	0.6	0.54772256	2.776	0.680		1.8	1.0954451	2.776	1.360
0.2	1	1	2.776	1.241		1.6	0.54772256	2.776	0.680
0.25	1.2	0.4472136	2.776	0.555		0.6	0.89442719	2.776	1.110
0.3	1.6	0.54772256	2.776	0.680		1.2	1.0954451	2.776	1.360
0.4	0.6	0.89442719	2.776	1.110		1	1	2.776	1.241
0.5	0.2	0.4472136	2.776	0.555		0.6	0.54772256	2.776	0.680

Figure A-1: Uncertainty Calculations.

Appendix B

Raw Data

B.1 1992- Courtesy of Kurt Roth

This data was taken by Kurt Roth during the summer of 1992. Notice that the number of photos examined for each case was not the same so that the count had to be normalized as shown in figure B-5. The size of each particle and the total number of particles were recorded for each diameter range.

B.2 1993

The data collected in 1993 starts on page 66. Table B.1 gives the corresponding location in the test section for each photo number.

Location	Photo Number
no step	1, 2, 4, 5
x/h = 3	12, 13, 14, 16
x/h = 6	11, 15, 17, 18, 19
x/h = 9	6, 7, 8, 9, 10

Table B.1: Corresponding Location in Test Section for Photo Number.

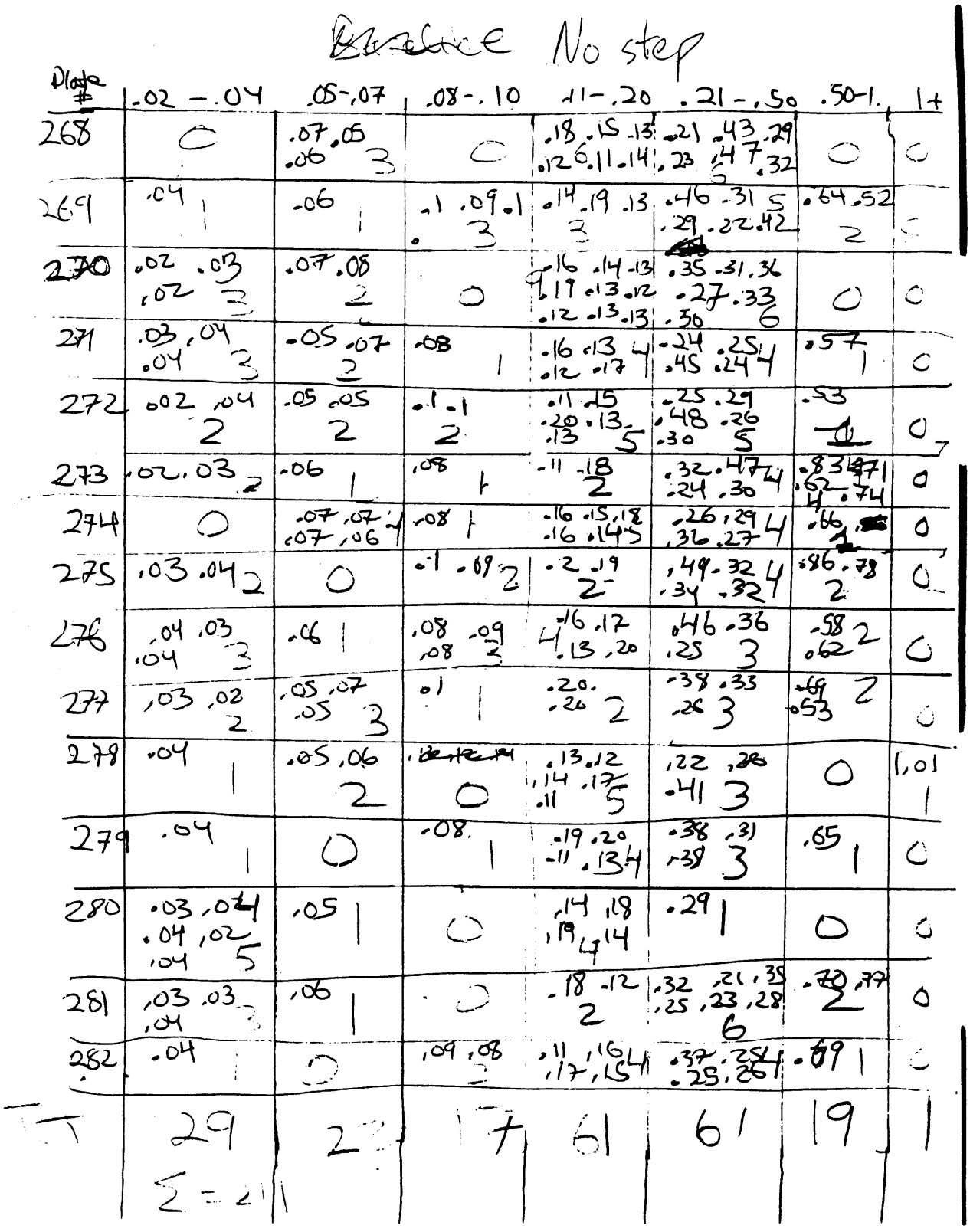

Figure B-1: Particle Sizing and Counting- No Step, 1992.

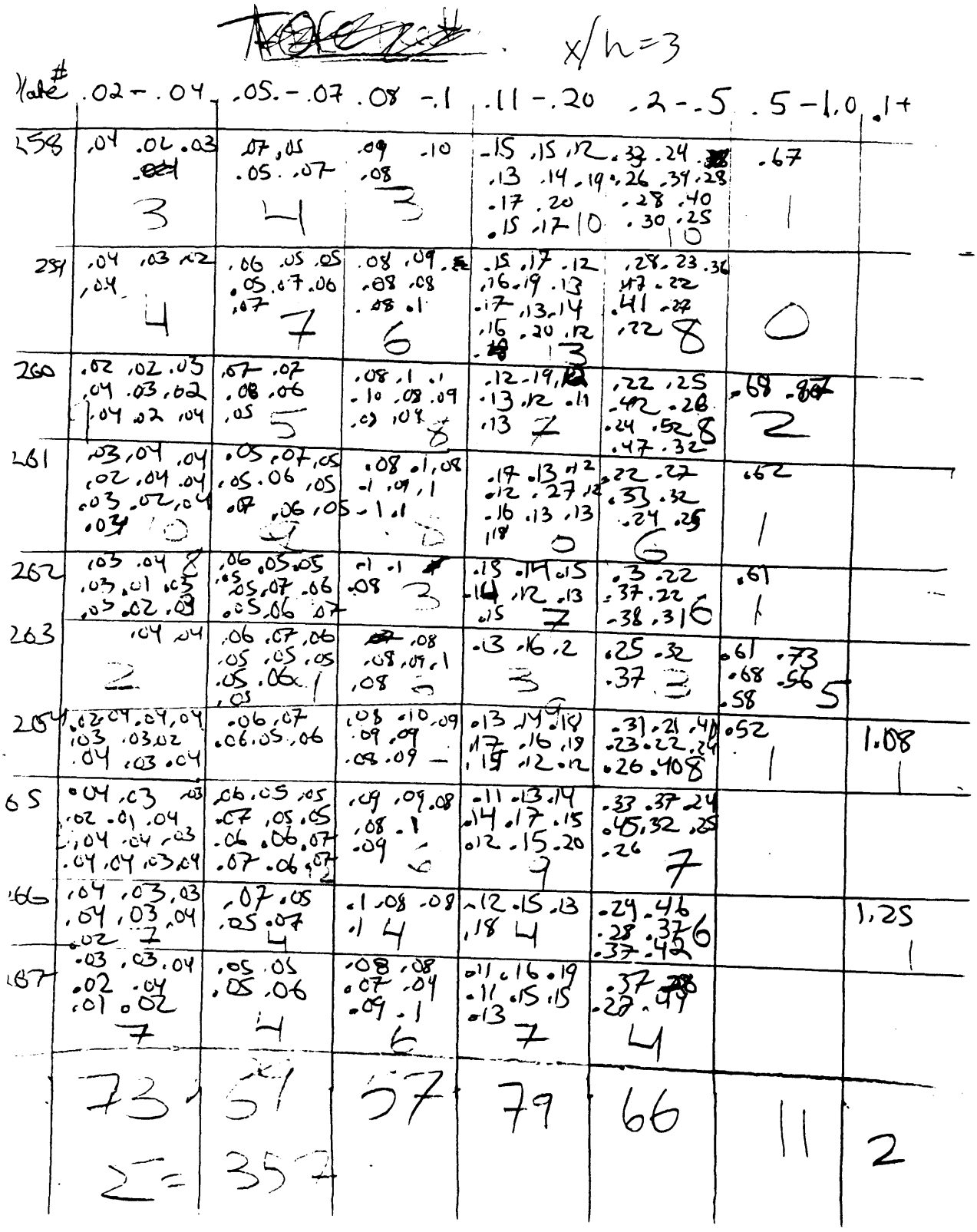

Figure B-2: Particle Sizing and Counting- x/h = 3, 1992.

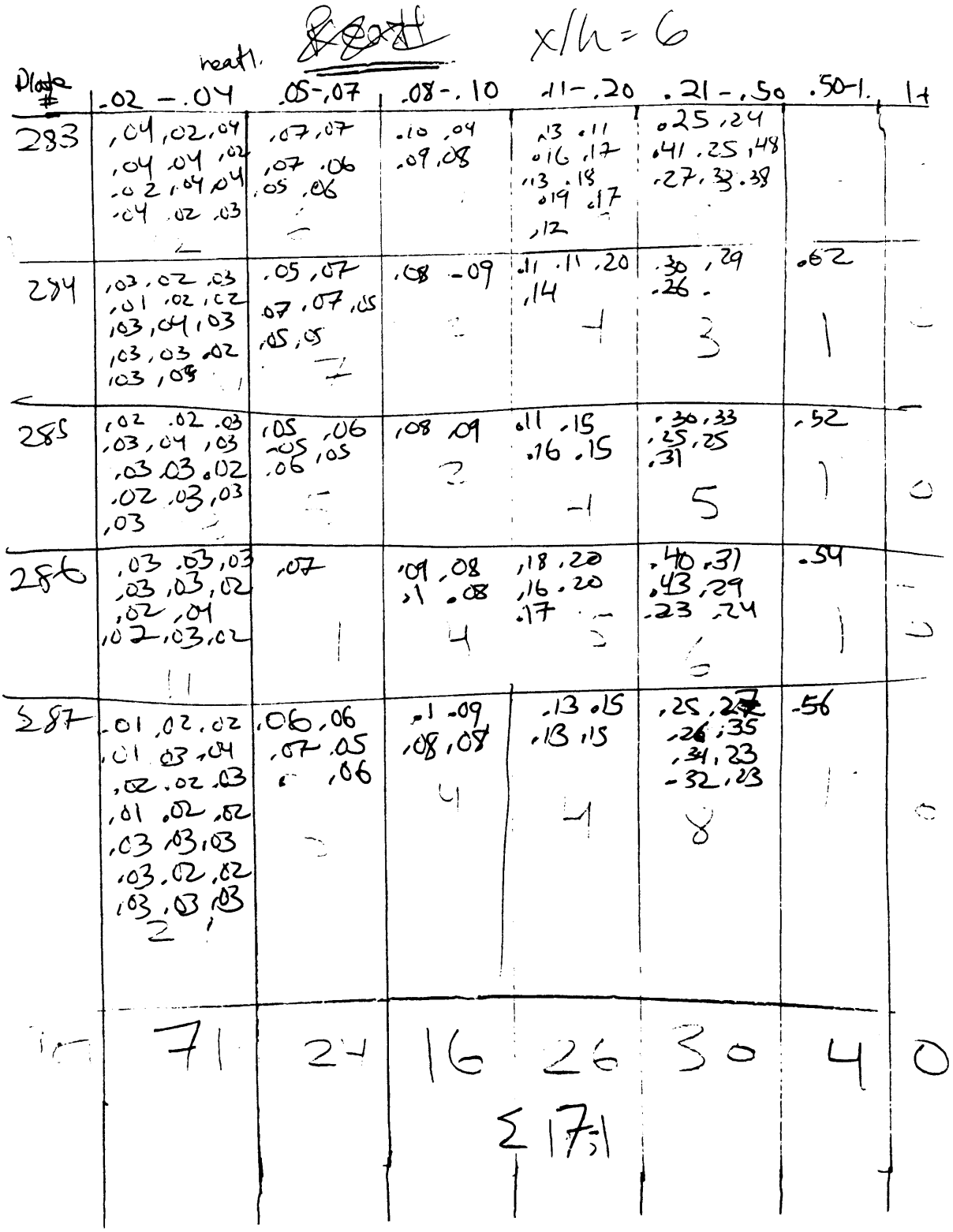

Figure B-3: Particle Sizing and Counting- x/h = 6, 1992.

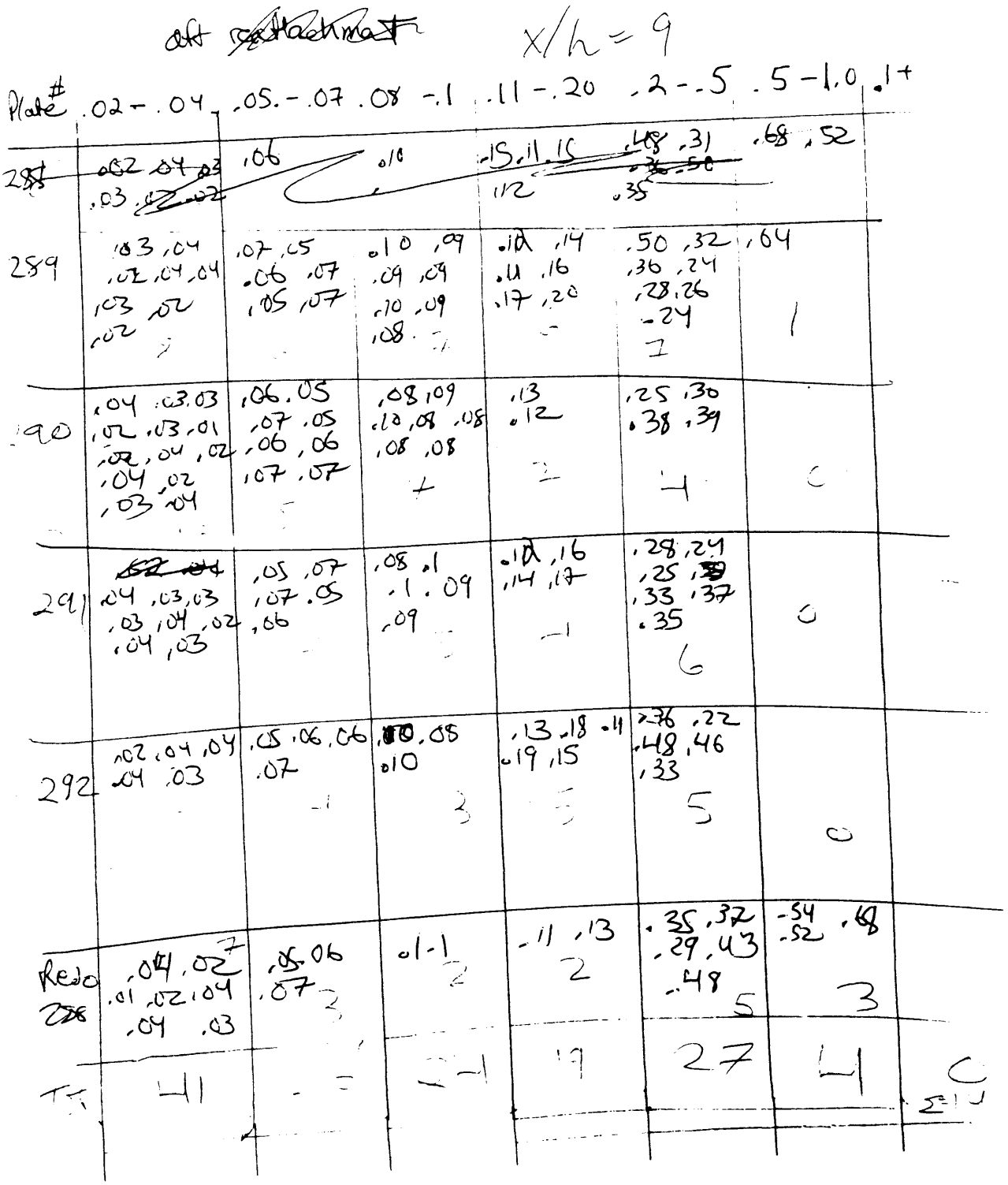

Figure B-4: Particle Sizing and Counting- x/h = 9, 1992.

Plate #	.02 - .04	.05 - .07	.08 - .10	.11 - .20	.21 - .50	.50 - 1.	1+
X/n=3 [illegible]	73	6[illegible]	57	7[illegible]	66	11	2
3-1-Q	122	57	35	49	60	7	2
[illegible] 9 TOT=272	52	45	40	36	39	8	2
Si-Cine TOT=259	33	32	24	70	74	24	2

	# particles sampled	[illegible]	20kX ~5μ X 3.4.
X/n-2	10	5.2	
X/n-6	10	8.2	
X/n-4	10	8.2	
[illegible]	20	14.4	

Figure B-5: Particle Sizing and Counting- Totals, 1992.

onebin.tiff(Measurements)

Area	Perimeter		Diameter(A)	Diameter(P)
0.00004067	0.01803861		0.00719784	0.00574478
0.00004067	0.01803861		0.00719784	0.00574478
0.00004067	0.01803861		0.00719784	0.00574478
0.00004067	0.01803861		0.00719784	0.00574478
0.00008135	0.03079383		0.01017991	0.00980695
0.00008135	0.03079383		0.01017991	0.00980695
0.0001627	0.05630427		0.01439657	0.0179313
0.0001627	0.05630427		0.01439657	0.0179313
0.0001627	0.05630427		0.01439657	0.0179313
0.0001627	0.03607721		0.01439657	0.01148956
0.0001627	0.03607721		0.01439657	0.01148956
0.0001627	0.03607721		0.01439657	0.01148956
0.00020337	0.06905949		0.01609565	0.02199347
0.00032539	0.10732516		0.02035951	0.03417999
0.00048809	0.07215443		0.02493533	0.02297912
0.00048809	0.07215443		0.02493533	0.02297912
0.00056943	0.09766487		0.02693304	0.03110346
0.00061011	0.1966117		0.02787849	0.06261519
0.00065078	0.08490965		0.02879269	0.02704129
0.00065078	0.08490965		0.02879269	0.02704129
0.00065078	0.08490965		0.02879269	0.02704129
0.00065078	0.08490965		0.02879269	0.02704129
0.00065078	0.08490965		0.02879269	0.02704129
0.00065078	0.08490965		0.02879269	0.02704129
0.00073213	0.23487736		0.03053931	0.07480171
0.00081348	0.10140079		0.03219131	0.03229325
0.00081348	0.10294826		0.03219131	0.03278607
0.00081348	0.09766487		0.03219131	0.03110346
0.00081348	0.09766487		0.03219131	0.03110346
0.00081348	0.09766487		0.03219131	0.03110346
0.00085415	0.12317532		0.0329862	0.03922781
0.00085415	0.09766487		0.0329862	0.03110346
0.00085415	0.09766487		0.0329862	0.03110346
0.00085415	0.09766487		0.0329862	0.03110346
0.00085415	0.09766487		0.0329862	0.03110346
0.0009355	0.11042009		0.03452129	0.03516563
0.00097617	0.11943939		0.0352637	0.03803802
0.00097617	0.11042009		0.0352637	0.03516563
0.00097617	0.11042009		0.0352637	0.03516563
0.00105752	0.11042009		0.03670367	0.03516563
0.00105752	0.11042009		0.03670367	0.03516563
0.00105752	0.11042009		0.03670367	0.03516563
0.00105752	0.11042009		0.03670367	0.03516563
0.00105752	0.11042009		0.03670367	0.03516563
0.00105752	0.11042009		0.03670367	0.03516563

3 pages

0.00113887	0.11943939		0.03808923	0.03803802
0.00117954	0.12208109		0.03876337	0.03887933
0.00126089	0.12317532		0.04007779	0.03922781
0.00126089	0.12317532		0.04007779	0.03922781
0.00130157	0.13593054		0.04071917	0.04328998
0.00130157	0.13593054		0.04071917	0.04328998
0.00130157	0.12317532		0.04071917	0.03922781
0.00138291	0.12845869		0.04197224	0.04091041
0.00138291	0.13593054		0.04197224	0.04328998
0.00146426	0.14230815		0.04318911	0.04532107
0.00162696	0.14868575		0.04552538	0.04735215
0.00178965	0.14649731		0.04774734	0.04665519
0.00223707	0.16672437		0.05338324	0.05309693
0.00227774	0.17464945		0.05386631	0.05562084
0.00227774	0.19642396		0.05386631	0.0625554
0.00248111	0.17574367		0.05621966	0.05596932
0.00272515	0.86252493		0.05891968	0.27468947
0.00300987	0.20763172		0.06192115	0.06612475
0.00313189	0.20917919		0.06316383	0.06661758
0.00345728	0.21400933		0.06636398	0.06815584
0.00361998	0.23250118		0.06790758	0.07404496
0.00361998	0.21819849		0.06790758	0.06948996
0.00366065	0.22193441		0.06828798	0.07067975
0.00382335	0.21929272		0.06978904	0.06983845
0.00394537	0.26812515		0.07089393	0.08539018
0.00414874	0.24525639		0.07269814	0.07810713
0.00418941	0.23204793		0.0730536	0.07390061
0.00459615	0.24635063		0.07651776	0.07845561
0.00553165	0.27031359		0.08394455	0.08608713
0.00662985	0.3052966		0.09190032	0.09722822
0.00667052	0.29737151		0.09218176	0.0947043
0.00723996	0.32442942		0.09603582	0.10332147
0.00740265	0.31959927		0.09710884	0.10178321
0.00756535	0.3233352		0.0981702	0.10297299
0.00837883	0.33609042		0.10331345	0.10703517
0.01399183	0.4418681		0.13350651	0.14072232
0.01598485	0.50809819		0.14269852	0.16181471
0.01785585	0.50281477		0.15081878	0.16013209
0.01895405	0.51028663		0.15538754	0.16251167
0.02115044	0.59957319		0.16414395	0.19094688
0.02143515	0.54791129		0.16524504	0.17449404
0.02265537	0.55602413		0.16988332	0.17707775
0.02359087	0.59674376		0.17335531	0.19004578
0.02477042	0.58617699		0.17763636	0.18668057
0.04628692	0.80018628		0.24282551	0.25483639
0.0469377	0.80392224		0.24452658	0.25602619

79 in b7

10 in B2

2 in B3

0.11559527	1.28915167		0.38373835	0.41055786
0.23293953	1.80117345		0.54473687	0.57362212

1 in B4
1 in B6

93 in total

Area	Perimeter Length		Diameter(A)	Diameter(P)		
0.00015776	0.04043139		0.01417273	0.012869711		
0.00019282	0.05227347		0.015668633	0.016639162		
0.00021035	0.04880501		0.016365388	0.015535117		
0.00021035	0.04880501		0.016365388	0.015535117		
0.00028047	0.06238132		0.018897235	0.019856591		
0.00028047	0.05574194		0.018897235	0.017743211		
0.00028047	0.05574194		0.018897235	0.017743211		Photo
0.00033306	0.06166298		0.020592843	0.019627936		Number
0.00036812	0.06411555		0.021649594	0.020408613		Two
0.00036812	0.06411555		0.021649594	0.020408613		
0.00036812	0.06411555		0.021649594	0.020408613		
0.00040318	0.07422341		0.022657112	0.023626045		
0.00045576	0.07248917		0.024089244	0.023074019		
0.00045576	0.07248917		0.024089244	0.023074019		67 in total
0.00045576	0.07494175		0.024089244	0.0238547		
0.00047329	0.07841021		0.024548147	0.024958745		
0.00047329	0.08504959		0.024548147	0.027072125		
0.00049082	0.08014444		0.024998629	0.025510768		
0.00049082	0.0794261		0.024998629	0.025282113		
0.00054341	0.08086278		0.026303823	0.025739422		
0.00056094	0.08086278		0.026724726	0.025739422		
0.00057847	0.0996418		0.027139102	0.03171697		
0.00057847	0.08779972		0.027139102	0.027947519		
0.00057847	0.0892364		0.027139102	0.028404828		
0.000596	0.0892364		0.027547246	0.028404828		
0.000596	0.0892364		0.027547246	0.028404828		
0.00061353	0.08678383		0.02794943	0.027624151		
0.00063106	0.0944391		0.028345909	0.030060899		
0.00066612	0.09372076		0.029122677	0.029832244		
0.00070117	0.09761002		0.029879046	0.031070234		
0.00073623	0.09617333		0.030616942	0.030612922		
0.00084141	0.10454695		0.032730971	0.033278328		
0.00084141	0.10454695		0.032730971	0.033278328		
0.000894	0.10454695		0.033738348	0.033278328		
0.0010167	0.11292057		0.035979197	0.035943734		
0.0010167	0.11292057		0.035979197	0.035943734		
0.0010167	0.12057584		0.035979197	0.038380482		
0.00105176	0.12302841		0.036594295	0.039161159		
0.00106929	0.1240443		0.036897999	0.039484527		
0.00106929	0.12129418		0.036897999	0.038609137		
0.00112188	0.1240443		0.03779447	0.039484527		

0.00122706	0.12649688		0.039526463	0.040265207		
0.00133223	0.1348705		0.04118553	0.042930614		
0.00152505	0.14988349		0.044065337	0.047709397		
0.00154258	0.14396246		0.044317873	0.045824674		
0.00166529	0.15161772		0.046046857	0.048261419		
0.00166529	0.15652279		0.046046857	0.049822751		
0.00178799	0.15580453		0.047713096	0.049594122		
0.00226129	0.17356765		0.053657841	0.055248299		
0.00238399	0.17775446		0.055094377	0.056581002		
0.00264693	0.2184834		0.058053217	0.069545426		
0.00303258	0.20317286		0.062138561	0.06467193		
0.00529387	0.28619066		0.082099724	0.091097316		
0.00548669	0.27709872		0.083581521	0.088203262		
0.00620539	0.2931276		0.088887277	0.093305413		
0.00622292	0.29659608		0.08901274	0.094409464		
0.00629304	0.3217169		0.089512834	0.10240567		
0.00709939	0.31232741		0.095074834	0.099416902		
0.00744998	0.32518539		0.097394092	0.10350972		
0.01130644	0.40503228		0.11998253	0.12892578		
0.01151679	0.43607417		0.12109349	0.13880672		
0.01791501	0.49570537		0.15103013	0.15778792		
0.03602283	0.71460956		0.21416277	0.22746729		
0.074710131	0.04051328		0.30842162	0.012895778		
0.091065031	0.15977573		0.34051079	0.050858194		
0.14328499	0.41911125		0.42712541	0.13340725		
0.17255902	0.61492646		0.46873123	0.19573717		

3 in
1 in
2 in
2 in

photo # 2

Area	Perimeter Length		Diameter(A)	Diameter(P)	
1.861e-05			0.0048677498		
1.861e-05			0.0048677498		
3.721e-05			0.0068831129		
9.303e-05			0.01088345		
0.00011163			0.011921901		
0.00013024			0.012877372		
0.00014884			0.013766226		Photo
0.00016745			0.014601505		Number
0.00020466			0.016142528		Four
0.00026048			0.018211355		
0.00029769			0.01946871		81 in total
0.00029769			0.01946871		
0.0003163			0.020068026		
0.00035351			0.021215629		
0.00035351			0.021215629		
0.00039072			0.022304263		
0.00039072			0.022304263		
0.00042793			0.023342181		
0.00046514			0.024335872		
0.00046514			0.024335872		
0.00048375			0.02481793		
0.00048375			0.02481793		
0.00053956			0.026210477		
0.00055817			0.026658659		
0.00057677			0.027099195		
0.00057677			0.027099195		
0.00057677			0.027099195		
0.00057677			0.027099195		
0.00059538			0.027532914		
0.00059538			0.027532914		
0.00059538			0.027532914		
0.00059538			0.027532914		
0.00061398			0.027959678		
0.00063259			0.02838025		
0.0006698			0.029203011		
0.0006698			0.029203011		
0.0006698			0.029203011		
0.0006698			0.029203011		
0.00068841			0.029605926		
0.00068841			0.029605926		
0.00068841			0.029605926		
0.00074422			0.03078263		
0.00078143			0.03154279		
0.00081865			0.032285253		
0.00091167			0.034070138		
0.00093028	0.11738198		0.03441612	0.037363845	
0.00093028			0.03441612		
0.00111634			0.037701038		
0.00117215			0.038631952		
0.00145124			0.042985767		
0.00150705			0.043804516		
0.00156287			0.044608384		
0.00163729			0.045658103		
0.0019908			0.050346453		
0.00280944			0.05980878		
0.00293968			0.061179382		

0.00351646			0.066912599			
0.00446534			0.075401906			
0.00461419			0.076648348			
0.00807483			0.10139622			
0.01036331			0.11486939			
0.01092148			0.11792226			
0.01224248			0.12485035			
0.01428909			0.13488304			
0.01655898			0.14520175			
0.01657758			0.14528328			
0.01767531			0.15001634			
0.01877304			0.15460458			
0.02145225			0.16526903			
0.02439193			0.17622931			
0.0246338			0.1771009			
0.02478265			0.17763516			
0.02584317			0.1813961			
0.03242955			0.20320085			
0.03581576			0.21354635			
0.04750007			0.24592472			
0.04984438			0.2519203			
0.05514697			0.2649817			
0.05864482			0.27325611			
0.06973375			0.29797276			
0.14904939			0.43563239			

59 in B1

14 in B2

photo #4

7 in B3

1 in B5

fivebin.tiff(Measurements)

Area	Perimeter		Diameter(A)	Diameter(P)
0.00006654	0.02307176		0.00920675	0.00734769
0.00013308	0.03938597		0.01302032	0.0125433
0.00013308	0.03938597		0.01302032	0.0125433
0.00019961	0.04614353		0.01594617	0.01469539
0.00026615	0.04614353		0.01841316	0.01469539
0.00026615	0.04614353		0.01841316	0.01469539
0.00026615	0.04614353		0.01841316	0.01469539
0.00026615	0.06245773		0.01841316	0.019891
0.00033269	0.06245773		0.02058662	0.019891
0.00033269	0.06245773		0.02058662	0.019891
0.00039923	0.06245773		0.02255157	0.019891
0.00059884	0.07877193		0.0276198	0.0250866
0.00059884	0.08552949		0.0276198	0.02723869
0.00059884	0.07877193		0.0276198	0.0250866
0.00059884	0.08552949		0.0276198	0.02723869
0.00059884	0.07877193		0.0276198	0.0250866
0.00066538	0.10044416		0.02911388	0.03198859
0.00066538	0.09228706		0.02911388	0.02939078
0.00066538	0.08552949		0.02911388	0.02723869
0.00073192	0.10184369		0.03053493	0.0324343
0.00073192	0.10184369		0.03053493	0.0324343
0.00073192	0.10184369		0.03053493	0.0324343
0.00073192	0.09030781		0.03053493	0.02876045
0.00073192	0.09706537		0.03053493	0.03091254
0.00079846	0.09508613		0.03189273	0.03028221
0.00079846	0.09508613		0.03189273	0.03028221
0.00079846	0.10184369		0.03189273	0.0324343
0.00079846	0.09228706		0.03189273	0.02939078
0.00079846	0.09508613		0.03189273	0.03028221
0.00079846	0.09508613		0.03189273	0.03028221
0.00079846	0.09508613		0.03189273	0.03028221
0.00079846	0.09228706		0.03189273	0.02939078
0.00079846	0.09508613		0.03189273	0.03028221
0.000865	0.09706537		0.03319504	0.03091254
0.00093154	0.11815789		0.03444815	0.0376299
0.00093154	0.11815789		0.03444815	0.0376299
0.00093154	0.11815789		0.03444815	0.0376299
0.00099807	0.10662201		0.03565707	0.03395605
0.00106461	0.10860126		0.0368265	0.03458639
0.00106461	0.11337958		0.0368265	0.03610815
0.00106461	0.10860126		0.0368265	0.03458639
0.00106461	0.10860126		0.0368265	0.03458639
0.00106461	0.10860126		0.0368265	0.03458639
0.00106461	0.10860126		0.0368265	0.03458639
0.00106461	0.10860126		0.0368265	0.03458639

3 pgs

	0.00106461	0.10860126		0.0368265	0.03458639
	0.00106461	0.10860126		0.0368265	0.03458639
	0.00106461	0.10860126		0.0368265	0.03458639
	0.00106461	0.10860126		0.0368265	0.03458639
	0.00106461	0.10860126		0.0368265	0.03458639
	0.00106461	0.10860126		0.0368265	0.03458639
	0.00106461	0.10860126		0.0368265	0.03458639
	0.00106461	0.10860126		0.0368265	0.03458639
	0.00106461	0.10860126		0.0368265	0.03458639
	0.00106461	0.10860126		0.0368265	0.03458639
	0.00106461	0.10860126		0.0368265	0.03458639
	0.00119769	0.11815789		0.03906046	0.0376299
	0.00119769	0.14938676		0.03906046	0.0475754
	0.00133077	0.12491546		0.04117339	0.03978199
	0.00133077	0.12491546		0.04117339	0.03978199
	0.00133077	0.12491546		0.04117339	0.03978199
	0.00133077	0.12491546		0.04117339	0.03978199
	0.0013973	0.12969378		0.04219005	0.04130375
	0.0013973	0.12491546		0.04219005	0.03978199
	0.0013973	0.12491546		0.04219005	0.03978199
	0.00146384	0.12969378		0.04318292	0.04130375
	0.00173	0.14122966		0.04694488	0.0449776
	0.00173	0.14122966		0.04694488	0.0449776
	0.00186307	0.15754387		0.04871691	0.05017321
	0.00212923	0.1595231		0.05208066	0.05080354
	0.00306076	0.19890907		0.06244243	0.06334684
	0.00339345	0.20846571		0.06574851	0.06639035
	0.0039923	0.23153748		0.07131432	0.07373805
	0.00419191	0.23153748		0.07307539	0.07373805
	0.00432499	0.23969458		0.07422629	0.07633585
	0.00565575	0.2737225		0.08488096	0.08717277
77	0.00598845	0.29061642		0.08734185	0.092553
78	0.00612152	0.29061642		0.08830693	0.092553
79	0.00825075	0.33675995		0.10252078	0.10724839
	0.00825075	0.32464436		0.10252078	0.10338992
81	0.00878305	0.33955902		0.10577617	0.10813982
	0.00931536	0.35785246		0.10893439	0.11396575
83	0.01018036	0.37894499		0.11387981	0.12068312
	0.01037997	0.38570255		0.11499083	0.12283521
85	0.01191035	0.41355264		0.12317638	0.13170466
	0.01257574	0.4203102		0.12657034	0.13385675
87	0.01270881	0.41833097		0.12723823	0.13322642
	0.01330766	0.42986685		0.13020151	0.13690027
89	0.01417266	0.44338197		0.13436645	0.14120445
	0.01417266	0.43662441		0.13436645	0.13905236
91	0.01470496	0.45293862		0.13686648	0.14424797

78 in B1

fivebin.tiff(Measurements)

0.02368763	0.5657385		0.17371046	0.1801715
0.0250184	0.59416825		0.17852331	0.18922556
0.02614955	0.60570413		0.18251446	0.1928994
0.027813	0.61724001		0.18823011	0.19657325
0.03446683	0.6892544		0.20953947	0.21950777
0.04444758	0.77758294		0.23795193	0.24763788
0.05875331	0.90727675		0.27357811	0.28894164
0.05961831	0.94468343		0.27558464	0.3008546

19

17 in B2

4 in B3

99 in total

twelve.tiff(Measurements)

Area	Perimeter		Diameter(A)	Diameter(P)
0.00028413	0.04767607		0.01902496	0.01518346
0.00028413	0.04767607		0.01902496	0.01518346
0.00028413	0.04767607		0.01902496	0.01518346
0.00028413	0.04767607		0.01902496	0.01518346
0.00028413	0.04767607		0.01902496	0.01518346
0.00028413	0.04767607		0.01902496	0.01518346
0.00028413	0.04767607		0.01902496	0.01518346
0.00035516	0.0645321		0.02127048	0.02055162
0.00049722	0.08138814		0.02516746	0.02591979
0.00056825	0.08837014		0.02690512	0.02814336
0.00056825	0.09679815		0.02690512	0.03082744
0.00063928	0.08138814		0.02853716	0.02591979
0.00063928	0.09535214		0.02853716	0.03036692
0.00063928	0.08138814		0.02853716	0.02591979
0.00071031	0.09679815		0.03008078	0.03082744
0.00078135	0.10522617		0.03154917	0.03351152
0.00085238	0.09824417		0.032952	0.03128795
0.00085238	0.10028915		0.032952	0.03193922
0.00085238	0.10871717		0.032952	0.0346233
0.00085238	0.09824417		0.032952	0.03128795
0.00085238	0.11714519		0.032952	0.03730739
0.00085238	0.09535214		0.032952	0.03036692
0.00085238	0.09535214		0.032952	0.03036692
0.00099444	0.14447422		0.03559217	0.0460109
0.00106547	0.11714519		0.03684137	0.03730739
0.0011365	0.11714519		0.03804958	0.03730739
0.00127857	0.12412719		0.04035779	0.03953095
0.00156269	0.14098322		0.04461713	0.04489911
0.00241507	0.16975828		0.05546641	0.05406315
0.00284126	0.20900632		0.06016178	0.06656252
0.00369364	0.21045233		0.068595	0.06702304
0.00419086	0.24970038		0.07306624	0.07952241
0.00525633	0.28136748		0.08182886	0.08960748
0.00617974	0.29039446		0.08872587	0.09248231
0.01392217	0.43367076		0.13317375	0.13811171
0.03253242	0.66447014		0.20357449	0.21161469
0.04432364	0.78655231		0.23761994	0.25049437
0.04567324	0.78655231		0.24121043	0.25049437
0.06939775	0.99086976		0.29732941	0.31556362
0.09724209	1.18651104		0.35195919	0.37786976
0.15896845	1.48413563		0.45000842	0.47265466

1 pixel

41 in total

34 in bin 1
1 in bin 2
3 in bin 3
2 in b4
1 in b5

.001 mm – 1 mm

thirteen.tiff(Measurements)

Area	Perimeter		Diameter(A)	Diameter(P)
0.00007076	0.02379213		0.00949422	0.00757711
0.00007076	0.02379213		0.00949422	0.00757711
0.00007076	0.02379213		0.00949422	0.00757711
0.00007076	0.02379213		0.00949422	0.00757711
0.00007076	0.02379213		0.00949422	0.00757711
0.00007076	0.02379213		0.00949422	0.00757711
0.00007076	0.02379213		0.00949422	0.00757711
0.00007076	0.02379213		0.00949422	0.00757711
0.00007076	0.02379213		0.00949422	0.00757711
0.00014152	0.04409998		0.01342685	0.01404458
0.00014152	0.04061571		0.01342685	0.01293494
0.00014152	0.04409998		0.01342685	0.01404458
0.00014152	0.04409998		0.01342685	0.01404458
0.00014152	0.04061571		0.01342685	0.01293494
0.00014152	0.04061571		0.01342685	0.01293494
0.00021227	0.04758426		0.01644408	0.01515422
0.00021227	0.04758426		0.01644408	0.01515422
0.00021227	0.04758426		0.01644408	0.01515422
0.00028303	0.04758426		0.0189881	0.01515422
0.00028303	0.04758426		0.0189881	0.01515422
0.00028303	0.04758426		0.0189881	0.01515422
0.00035379	0.07137639		0.02122941	0.02273133
0.00035379	0.06440783		0.02122941	0.02051205
0.00035379	0.06789211		0.02122941	0.02162169
0.00049531	0.0763039		0.02511908	0.02430061
0.00056607	0.09661175		0.02685346	0.03076807
0.00070758	0.09312747		0.03002292	0.02965843
0.0008491	0.10009603		0.03288854	0.03187772
0.00134441	0.12388816		0.04138386	0.03945483
0.00134441	0.14419602		0.04138386	0.0459223
0.00141516	0.12881567		0.04245882	0.0410241
0.00148592	0.14071174		0.04350738	0.04481266
0.00198123	0.15753531		0.05023803	0.05017048
0.00212275	0.16246283		0.05200135	0.05173975
0.00226426	0.16739033		0.05370668	0.05330902
0.00240578	0.17639993		0.05535962	0.05617832
0.00247654	0.17435889		0.05616786	0.05552831
0.00268881	0.19118246		0.05852551	0.06088613
0.00353791	0.21845888		0.06713339	0.06957289
0.00467004	0.26255885		0.07713038	0.08361747
0.00813719	0.33537847		0.1018128	0.10680843
0.01125055	0.39281777		0.11971596	0.1251012
0.01436391	0.43836099		0.13527001	0.13960541
0.01492998	0.45025703		0.13790969	0.14339396
0.01868016	0.5195924		0.15426076	0.16547529

2 pages

51 in total

40 in bin 1

5 in bin 2

thirteen.tiff(Measurements)

0.04103974	0.74442202		0.22864803	0.23707708
0.04118126	0.75631809		0.22904193	0.24086563
0.06403615	0.93560445		0.28561287	0.2979632
0.0903582	1.11981833		0.33927273	0.35663004
0.12460516	1.31592834		0.39841271	0.41908546
0.13656329	1.37829518		0.41709229	0.43894751

3 in bin-3
1 in b4
2 in b5

sixteen.tiff(Measurements)

Area	Perimeter		Diameter(A)	Diameter(P)
0.00003777	0.01738189		0.00693647	0.00553563
0.0001133	0.03476378		0.01201379	0.01107127
0.00015107	0.03476378		0.01387249	0.01107127
0.00018883	0.04705463		0.0155096	0.01498555
0.0002266	0.04705463		0.01699007	0.01498555
0.0002266	0.04705463		0.01699007	0.01498555
0.0002266	0.06803641		0.01699007	0.02166765
0.00030213	0.05574557		0.01961833	0.01775337
0.00030213	0.05574557		0.01961833	0.01775337
0.0003399	0.05934548		0.0208085	0.01889983
0.0003399	0.06443651		0.0208085	0.02052118
0.0003399	0.05934548		0.0208085	0.01889983
0.00037766	0.07058194		0.02193389	0.02247832
0.0004532	0.07163633		0.02402758	0.02281412
0.0004532	0.07163633		0.02402758	0.02281412
0.0004532	0.06952755		0.02402758	0.02214253
0.0004532	0.06952755		0.02402758	0.02214253
0.0004532	0.06952755		0.02402758	0.02214253
0.00052873	0.08796383		0.02595268	0.02801396
0.00060426	0.0818184		0.02774451	0.02605682
0.00075533	0.09410925		0.03101941	0.0299711
0.00079309	0.09410925		0.03178531	0.0299711
0.00079309	0.09770916		0.03178531	0.03111757
0.00094416	0.1064001		0.03468071	0.03388538
0.00105745	0.11149114		0.03670245	0.03550673
0.00147288	0.14581817		0.04331605	0.04643891
0.00154842	0.13607283		0.04441294	0.0433353
0.00192608	0.16109128		0.04953388	0.05130296
0.00215268	0.17338213		0.05236666	0.05521724
0.00222821	0.21789123		0.05327743	0.06939211
0.00226597	0.1754909		0.05372696	0.05588882
0.00241704	0.18312746		0.05548902	0.05832085
0.00249257	0.17803642		0.05634934	0.0566995
0.00339896	0.20981793		0.06580186	0.066821
0.00373886	0.22254553		0.06901361	0.07087437
0.00419205	0.23992741		0.07307661	0.07641
0.00506068	0.26196361		0.08029151	0.0834279
0.01253839	0.41138166		0.12638224	0.13101327
0.01593736	0.46712723		0.14248638	0.14876663
0.01695705	0.48301801		0.14697394	0.15382739
0.02062037	0.53007263		0.16207402	0.16881294
0.02254645	0.55974537		0.16947446	0.17826286
0.0276449	0.62629062		0.18766042	0.19945561
0.03466942	0.69941813		0.21015439	0.22274463
0.03561357	0.69327265		0.21299673	0.22078747

2 pages

48 in total

37 in bin 1

6 in bin 2

2 in bin 3

0.10804924	1.23203623		0.37100181	0.39236823	2 in b4
0.10846467	1.24072719		0.37171434	0.39513605	
0.23758748	1.82312644		0.55014472	0.58061352	1 in b6

fourteen.tiff(Measurements)

Area	Perimeter		Diameter(A)	Diameter(P)
0.0000652	0.02283839		0.00911358	0.00727337
0.0001304	0.03898757		0.01288855	0.01241642
0.0002608	0.04567679		0.01822716	0.01454675
0.0002608	0.04567679		0.01822716	0.01454675
0.0002608	0.04567679		0.01822716	0.01454675
0.0002608	0.04567679		0.01822716	0.01454675
0.0002608	0.04567679		0.01822716	0.01454675
0.000326	0.06851517		0.02037858	0.02182012
0.00039119	0.06182597		0.02232333	0.0196898
0.00039119	0.06182597		0.02232333	0.0196898
0.00039119	0.06182597		0.02232333	0.0196898
0.00039119	0.08466436		0.02232333	0.02696317
0.00052159	0.07324516		0.02577685	0.02332648
0.00052159	0.08466436		0.02577685	0.02696317
0.00052159	0.07797515		0.02577685	0.02483285
0.00058679	0.07797515		0.0273405	0.02483285
0.00078239	0.09135357		0.03157016	0.02909349
0.00104318	0.11223274		0.03645397	0.03574291
0.00104318	0.11557734		0.03645397	0.03680807
0.00110838	0.11696272		0.03757591	0.03724927
0.00117358	0.11892195		0.03866531	0.03787323
0.00130398	0.12365194		0.04075685	0.0393796
0.00143438	0.13034114		0.04274618	0.04150992
0.00143438	0.13507113		0.04274618	0.04301628
0.00149958	0.14176033		0.0437069	0.0451466
0.00149958	0.13507113		0.0437069	0.04301628
0.00176037	0.14649032		0.04735514	0.04665297
0.00202117	0.15595029		0.05074188	0.0496657
0.00202117	0.16263951		0.05074188	0.05179602
0.00221677	0.17209949		0.05314048	0.05480875
0.00228197	0.17209949		0.05391631	0.05480875
0.00241236	0.17405871		0.05543528	0.05543271
0.00254276	0.17878869		0.05691384	0.05693907
0.00273836	0.18351868		0.05906231	0.05844544
0.00286876	0.19297865		0.06045222	0.06145817
0.00371634	0.21973549		0.06880546	0.06997946
0.00541152	0.3219344		0.08302804	0.10252688
0.00547672	0.27291301		0.08352672	0.08691497
0.00567231	0.27821684		0.08500513	0.08860409
0.00854107	0.3380836		0.10430889	0.10766994
0.01193142	0.40602493		0.12328528	0.1293073
0.01264861	0.4188295		0.12693652	0.13338519
0.01864692	0.5101831		0.15412345	0.16247869
0.03657665	0.70316172		0.2158575	0.22393685
0.03775023	0.72127014		0.2192931	0.22970387

45

49 in total
2 pages

39 in line 1
4 in line 2

0.03846742	0.71931088		0.2213664	0.2290799
0.08593231	1.10053825		0.33085935	0.35048989
0.08886626	1.11864662		0.33646014	0.35625689
0.31634566	2.09887743		0.63481344	0.6684323

eleven.tiff(Measurements)

Area	Perimeter		Diameter(A)	Diameter(P)
0.0006236	0.08311713		0.02818501	0.02647042
0.00081847	0.09560309		0.03228989	0.03044684
0.00124719	0.12057498		0.03985947	0.03839968
0.00179284	0.15954763		0.04778988	0.05081135
0.00229951	0.17569062		0.05412312	0.05595243
0.00233848	0.16837652		0.05457981	0.0536231
0.00494979	0.26353592		0.07940696	0.08392864
0.06360675	0.93766946		0.28465366	0.29862085
0.07946946	1.07464731		0.31817445	0.34224437
0.44633853	2.50942874		0.75404517	0.79918113

2 in B1

1 in B3

1 in B4

1 in B5

10 in total

1 page

fifteen.tiff(Measurements)

Area	Perimeter		Diameter(A)	Diameter(P)
0.00006564	0.02291598		0.00914428	0.00729808
0.00019693	0.04583197		0.01583876	0.01459617
0.00019693	0.05393399		0.01583876	0.01717643
0.00026257	0.04583197		0.01828891	0.01459617
0.00026257	0.04583197		0.01828891	0.01459617
0.00032821	0.06539199		0.02044754	0.02082547
0.0004595	0.07349401		0.02419401	0.02340574
0.0004595	0.07349401		0.02419401	0.02340574
0.00052514	0.084952		0.02586442	0.02705478
0.00059079	0.07824007		0.02743353	0.02491722
0.00072207	0.08969805		0.03032877	0.02856626
0.00078771	0.09166393		0.03167731	0.02919233
0.00078771	0.09444411		0.03167731	0.03007774
0.00078771	0.09444411		0.03167731	0.03007774
0.00078771	0.09444411		0.03167731	0.03007774
0.000919	0.10115605		0.0342155	0.0322153
0.00098464	0.13217406		0.03541636	0.04209365
0.00098464	0.10786799		0.03541636	0.03435286
0.00098464	0.13553002		0.03541636	0.04316243
0.00105028	0.10786799		0.03657781	0.03435286
0.00118157	0.12407203		0.03879671	0.03951339
0.00131286	0.12881809		0.04089539	0.04102487
0.00144414	0.14027607		0.04289136	0.04467391
0.00210057	0.15648013		0.05172896	0.04983444
0.00210057	0.15648013		0.05172896	0.04983444
0.00288828	0.18610805		0.06065754	0.05927008
0.00288828	0.1908541		0.06065754	0.06078156
0.00630171	0.28055215		0.08959719	0.08934782
0.00899306	0.34872434		0.1070333	0.11105871
0.00912435	0.35208029		0.10781176	0.11212748
0.00912435	0.35486045		0.10781176	0.11301288
0.0145727	0.44988036		0.13624958	0.143274
0.01883948	0.50520444		0.1549172	0.16089313
0.02041491	0.5227986		0.16126455	0.16649637
0.05290809	0.8620308		0.25961287	0.2745321
0.05848773	0.90393102		0.27295909	0.28787612
0.09367226	1.14732897		0.34543845	0.36539139
0.09367226	1.14536309		0.34543845	0.36476532
0.14040993	1.39906752		0.42292571	0.4455629
0.15465441	1.48205364		0.44386032	0.47199161

40

1 page
28 in B1
6 in B2
2 in B3
2 in B4
2 in B5
40 Total

Area	Perimeter		Diameter(A)	Diameter(P)
0.00045504	0.06966884		0.02407631	0.02218753
0.00045504	0.0717819		0.02407631	0.02286048
0.00045504	0.0717819		0.02407631	0.02286048
0.00060672	0.08198467		0.02780093	0.02610977
0.00060672	0.08198467		0.02780093	0.02610977
0.00060672	0.08198467		0.02780093	0.02610977
0.00060672	0.08198467		0.02780093	0.02610977
0.00060672	0.08198467		0.02780093	0.02610977
0.00060672	0.08198467		0.02780093	0.02610977
0.0007584	0.09430049		0.03108238	0.030032
0.00079632	0.09430049		0.03184997	0.030032
0.00079632	0.09430049		0.03184997	0.030032
0.00079632	0.09430049		0.03184997	0.030032
0.00098592	0.10661632		0.03543937	0.03395424
0.00098592	0.10661632		0.03543937	0.03395424
0.00098592	0.10661632		0.03543937	0.03395424
0.00098592	0.10661632		0.03543937	0.03395424
0.00136512	0.12913491		0.0417014	0.04112577
0.00147888	0.13274214		0.04340419	0.04227457
0.0015168	0.14356381		0.04395713	0.04572096
0.00166848	0.14145073		0.04610263	0.045048
0.00197183	0.18455613		0.05011871	0.05877584
0.00204767	0.1860503		0.05107345	0.05925169
0.00227519	0.1660824		0.05383615	0.05289248
0.00231311	0.17479099		0.05428293	0.05566592
0.00291983	0.20813125		0.06098794	0.06628384
0.00295775	0.20707473		0.06138269	0.06594737
0.00436079	0.23786429		0.07453286	0.07575296
0.00697726	0.31219688		0.09427741	0.09942576
0.00792526	0.3608413		0.10047822	0.11491761
0.01308237	0.44643319		0.12909469	0.14217618
0.01547132	0.47616622		0.14038763	0.15164529
0.0167606	0.49420232		0.1461201	0.15738927
0.01922539	0.51417023		0.15649582	0.16374848
0.03154936	0.66961223		0.2004751	0.2132523
0.03230776	0.66899329		0.20287036	0.21305519
0.0522157	0.87413627		0.25790854	0.27838735
0.10621364	1.21923578		0.36783692	0.38829165
0.12430143	1.32224488		0.39792684	0.4210971

1 page

bin 1
29 in

5 in b2

3 in b3

1 in b4

1 in b5

39

39 in total

eighteen.tiff(Measurements)

Area	Perimeter		Diameter(A)	Diameter(P)
0.00019285	0.04755317		0.01567382	0.01514432
0.00050142	0.07390223		0.02527354	0.02353574
0.00061713	0.08268526		0.02803842	0.02633289
0.00077142	0.09510633		0.03134806	0.03028864
0.00080999	0.09510633		0.03212218	0.03028864
0.00080999	0.09510633		0.03212218	0.03028864
0.00088713	0.11524487		0.03361699	0.03670219
0.00096427	0.11116545		0.0350481	0.03540301
0.00111855	0.11994848		0.03774791	0.03820015
0.00123426	0.11994848		0.03965231	0.03820015
0.00131141	0.13236955		0.0408728	0.04215591
0.0015814	0.14629754		0.04488343	0.04659157
0.00262281	0.18764018		0.05780276	0.05975802
0.00636417	0.31637168		0.09004012	0.10075531
0.00998983	0.36969399		0.11280912	0.11773694
0.02514813	0.60080791		0.17898557	0.1913401
0.03911074	0.76529574		0.22320976	0.24372476
0.06969735	0.99703383		0.29797052	0.3175267
0.07494298	1.03819358		0.3089802	0.3306349
0.14564316	1.62845302		0.43073506	0.51861561

1 page

14 in b1

2 in b2

1 in b3

1 in b4

2 in b5

1 in b6

20 in total

Area	Perimeter Length		Diameter(A)	Diameter(P)	
0.0001191			0.012314334	0	
0.00047641	0.07497717		0.024628927	0.023865974	
0.00047641			0.024628927	0	
0.00055581			0.026602242	0	
0.00059551			0.02753592	0	
0.00063522			0.028439185	0	
0.00063522			0.028439185	0	Photo
0.00063522			0.028439185	0	Number
0.00063522			0.028439185	0	Nineteen
0.00063522			0.028439185	0	
0.00063522			0.028439185	0	~~81 in total~~ 45
0.00079402			0.031795875	0	
0.00079402			0.031795875	0	
0.00083372	0.26985636		0.032581057	0.085897947	
0.00083372			0.032581057	0	
0.00083372			0.032581057	0	
0.00083372			0.032581057	0	
0.00087342			0.033347757	0	
0.00103223			0.036252945	0	
0.00103223			0.036252945	0	
0.00103223			0.036252945	0	
0.00103223			0.036252945	0	
0.00123073			0.039585529	0	
0.00127043			0.040218922	0	
0.00134983			0.041456687	0	
0.00150864			0.043827618	0	
0.00154834	0.15472637		0.044400537	0.049250933	
0.00158804	0.14689665		0.044966158	0.046758656	
0.00158804			0.044966158	0	
0.00202475			0.050773928		
0.00226295			0.053677532	0	
0.00238206			0.055072071	0	
0.00254086			0.056878145	0	
0.00269967	0.19514149		0.058628718	0.062115465	
0.00341428			0.065933272	0	
0.00361279			0.06782291	0	
0.00559784			0.084423878	0	
0.01830214	0.50783741		0.15265323	0.16164967	
0.01925497			0.15657646	0	
0.02679815			0.18471726	0	
0.0371204			0.21740092	0	
0.04200362			0.23125888	0	
0.06336274			0.28403511	0	
0.080235651			0.31962353	0	
0.093019361	0.14303553		0.34414521	0.045529623	

photo #12

37 in B1

3 in B2

3 in B3

2 in B4

six.tiff(Measurements)

	Area	Perimeter		Diameter
1	0.00015873	0.04823332		0.01421984
2	0.00027777	0.05975125		0.01881082
3	0.00051587	0.07864934		0.02563512
4	0.00059523	0.10123752		0.02753643
5	0.00063491	0.09277656		0.02843945
6	0.00091269	0.11167465		0.03409784
	0.00091269	0.11428393		0.03409784
8	0.00099205	0.11905482		0.03554937
9	0.0011111	0.11644553		0.03762199
10	0.00123014	0.12688266		0.03958607
	0.00134919	0.1390337		0.04145737
12	0.00138887	0.14209068		0.04206259
13	0.00150792	0.15099932		0.04382827
14	0.00186505	0.15729863		0.04874279
15	0.00190474	0.16881661		0.04925871
16	0.00190474	0.16098878		0.04925871
17	0.0019841	0.18249615		0.05027441
18	0.00206346	0.15729868		0.05126999
19	0.00238092	0.19401407		0.05507285
20	0.00249997	0.22029234		0.05643293
	0.00253965	0.18096767		0.05687902
22	0.00317456	0.20769361		0.06359265
23	0.00361106	0.22029234		0.06782386
24	0.00365074	0.22029234		0.06819549
25	0.00392852	0.22703938		0.07074238
	0.00428566	0.23072946		0.07388802
	0.0044047	0.23963812		0.07490716
28	0.00515866	0.26591638		0.08106504
29	0.00555548	0.3130689		0.08412517
	0.00658721	0.29786089		0.09160431
31	0.00742053	0.32413915		0.09722605
32	0.00896813	0.41475409		0.10688484
33	0.01115064	0.40495008		0.11918321
34	0.01547598	0.49187496		0.14040878
35	0.02015845	0.5726859		0.16024841
36	0.03436461	0.70586795		0.20922852
	0.07456248	1.07671189		0.30819483
	0.20527498	1.71194375		0.51136757
	0.93546343	3.61745405		1.09163783

1 page

31 in B1

4 in B2

1 in B3

1 in B4

1 in B6

1 in B10

seven.tiff(Measurements)

	Area	Perimeter		Diameter
1	0.00124891	0.12917702		0.03988694
2	0.00396713	0.22198954		0.07108916
3	0.00429772	0.28657806		0.07399191
4	0.00554663	0.2840676		0.08405814
5	0.0071996	0.32649285		0.09576777
6	0.01068921	0.40467343		0.11669117
7	0.02064376	0.58631748		0.16216591
8	0.02350891	0.61852252		0.17305391
9	0.02464762	0.64355302		0.17719549
10	0.03592455	0.74224788		0.21392465
11	0.04382207	0.79428416		0.23627165
12	0.05594385	0.88458627		0.26695702
13	0.15042026	1.47341418		0.43774212
14	0.16687649	1.51834989		0.46106563

5 in B1

4 in B2

3 in B3

2 in B5

1 page

eight.tiff(Measurements)

	Area	Perimeter		Diameter(A)	Diameter(P)
1	0.00274349	0.18237524		0.05911761	0.05808129
2	0.00315501	0.19589926		0.06339654	0.0623883
3	0.00393233	0.22062695		0.07077667	0.07026336
4	0.0044353	0.25047591		0.07516691	0.0797694
5	0.0062643	0.3006109		0.08933085	0.09573596
6	0.00690444	0.30225164		0.09378414	0.09625848
7	0.00713307	0.29945073		0.09532425	0.09536647
8	0.00804756	0.32929969		0.10125052	0.10487251
9	0.00873343	0.35026532		0.10547696	0.11154946
10	0.01165982	0.4379724		0.12187401	0.13948166
11	0.01449476	0.49090832		0.13588474	0.15634023
12	0.0153178	0.48694724		0.13968937	0.15507874
13	0.01879289	0.53428131		0.15472552	0.17015328
14	0.02167355	0.56064975		0.16616142	0.17855088
15	0.03237315	0.67396319		0.20307556	0.21463796
16	0.06812993	0.97341388		0.29460095	0.31000442
17	0.06986748	1.01426744		0.29833397	0.32301511
18	0.12281679	1.29991269		0.39554331	0.41398493
19	0.24138117	1.82463098		0.55451955	0.58109267

7 in B1

7 in B2

3 in B3

1 in B4

1 in B6

1 page

nine.tiff(Measurements)

	Area	Perimeter		Diameter(A)	Diameter(P)
1	0.00185422	0.14911638		0.04860107	0.04748929
2	0.0021492	0.16209964		0.05232432	0.05162409
3	0.00455126	0.23777163		0.07614318	0.07572345
4	0.00522552	0.26642707		0.08158868	0.08484939
	0.00636333	0.28747708		0.09003418	0.09155321
	0.00809112	0.33894879		0.10152418	0.10794547
	0.0115467	0.39180452		0.12128138	0.12477851
	0.01639295	0.49567059		0.14450861	0.15785688
	0.01824716	0.50485116		0.15246242	0.16078062
	0.02452621	0.63180369		0.17675853	0.20121137
	0.03282804	0.68485051		0.20449733	0.21810526
	0.04020276	0.74262273		0.22630446	0.23650405
	0.07395791	1.03928041		0.30694283	0.33098102
	0.09157295	1.17068815		0.34154566	0.37283062
	0.12178823	1.33659053		0.39388354	0.42566577
	0.13325065	1.3717376		0.41200249	0.43685911
	0.26182362	1.90301657		0.5775234	0.60605623

5 in B1

4 in B2

3 in B3

2 in B4

2 in B5

1 in B7

1 page

ten.tiff(Measurements)

	Area	Perimeter		Diameter(A)	Diameter(P)
1	0.00161295	0.13907731		0.04532895	0.04429214
2	0.00186956	0.15118648		0.04880169	0.04814856
	0.00186956	0.15118648		0.04880169	0.04814856
	0.00190622	0.15118648		0.04927784	0.04814856
	0.00190622	0.15118648		0.04927784	0.04814856
	0.00219948	0.16329567		0.05293284	0.05200499
	0.00219948	0.16329567		0.05293284	0.05200499
	0.00219948	0.16329567		0.05293284	0.05200499
	0.00219948	0.16329567		0.05293284	0.05200499
	0.00252941	0.17540485		0.05676423	0.05586142
	0.00263938	0.19002192		0.05798506	0.06051654
	0.00263938	0.19002192		0.05798506	0.06051654
	0.0027127	0.19002192		0.05878494	0.06051654
	0.00293264	0.20213109		0.06112158	0.06437296
	0.00315259	0.19754559		0.06337222	0.06291261
16	0.00322591	0.21424027		0.06410491	0.06822939
17	0.00351917	0.20965476		0.06695535	0.06676903
18	0.00355583	0.20965476		0.06730319	0.06676903
	0.00421567	0.23387313		0.0732822	0.07448189
	0.0045456	0.2484902		0.07609582	0.07913701
	0.0045456	0.2484902		0.07609582	0.07913701
	0.0045456	0.2459823		0.07609582	0.07833831
	0.00498549	0.26059937		0.0796928	0.08299343
	0.00549871	0.27270854		0.08369424	0.08684985
	0.00729495	0.31655976		0.09639984	0.10081521
	0.00740492	0.36499646		0.09712373	0.11624091
	0.00784482	0.33117682		0.099967	0.10547032
	0.00879793	0.3412084		0.10586574	0.1086651
	0.00901788	0.36646557		0.1071809	0.11670878
	0.01964871	0.52933091		0.15820937	0.16857672
31	0.02049185	0.5343467		0.16156815	0.17017411
32	0.02148161	0.56358087		0.16542403	0.17948435
	0.02522073	0.62204915		0.17924374	0.19810482
	0.03097605	0.66339248		0.19864525	0.21127149
	0.03581491	0.74858701		0.21359796	0.23840351
36	0.03607152	0.70828247		0.2143618	0.22556767
37	0.11363994	1.28794944		0.38047898	0.41017498
38	0.12841313	1.34763479		0.4044547	0.42918305
39	0.16250511	1.5082444		0.45498668	0.48033261

27 in B1

7 in B2

2 in B3

1 in B4

2 in B5

Bibliography

[1] Aldrich Chemical, Inc. *Aldrich Chemical, Inc.-Catalog.*

[2] J. Colmenares. Measurements of the velocity response of inertial aerosols in grid-turbulence and in channel flow. S.M. Thesis in Mechanical Engineering, Massachusetts Institute of Technology, 1992.

[3] J.K. Eaton and J.P. Johnston. A review of research on subsonic turbulent flow reattachment. *American Institute of Aeronautics and Astronautics Journal*, 1981.

[4] J. Faramarzi and E. Logan. Reattachment length behind a single roughness element in turbulent pipe flow. *Journal of Fluids Engineering*, 1991.

[5] Sheldon Kay Friedlander. *Smoke, Dust, and Haze: Fundamentals of Aerosol Behavior.* Wiley, New York, 1977.

[6] Michael P. Frongillo. Personal communication to Michael Y. Feng, 1992.

[7] N.A. Fuchs. *The Mechanics of Aerosols.* Pergamon Press, New York, 1964.

[8] William C. Hinds. *Aerosol Technology: Properties, Behavior, and Measurement of Airborne Particles.* Wiley, New York, 1982.

[9] Kim, G.S., Lewars, G.G., Eldridge, M.A., and Sackner, M.A. Deposition of aerosol particles in a straight tube with an abrupt obstruction. *Journal of Aerosol Science*, 15(2):167–176, 1984.

[10] John H. Lienhard. *A Heat Transfer Textbook.* Prentice-Hall, Englewood Cliffs, New Jersey, second edition, 1987.

[11] John H. Lienhard V. Secondary flows and compound deposition mechanisms affecting ultrafine aerosol deposition in the lung. A proposal submitted to the National Institute of Environmental Health Sciences, August 1992.

[12] M.R. Maxey. The gravitational settling of aerosol particles in homogeneous turbulence and random flow fields. *Journal of Fluid Mechanics*, 174:441–465, 1987.

[13] P. Freymuth, W. Bank, and M. Palmer. Use of titanium tetrachloride for visualization of accelerating flow around airfoils. Technical report, University of Colorado, Boulder, year unknown.

[14] Merle C. Potter and John F. Foss. *Fluid Mechanics.* Great Lakes Press, Inc., Okemos, MI, 1982.

[15] Lenore Rainey. Personal communication to Michael Y. Feng, 1992.

[16] Ted Pella, Inc. *PELCO-Technical Note.*

[17] Ted Pella, Inc., Redding, CA. *Ted Pella, Inc.- Catalog 8*, 1991.